

CN 53-1040/Q ISSN 0254-5853

CODEN: DOYADI

ZOOLOGICAL RESEARCH

VOLUME 34 ISSUES E4-5
OCTOBER 2013



ZOOLOGICAL RESEARCH

Volume 34, Issues E4 – 5 October 2013

CONTENTS

The first mitochondrial genome for the butterfly family Riodinidae (*Abisara fylloides*) and its systematic implications

.....*Fang ZHAO, Dun-Yuan HUANG, Xiao-Yan SUN, Qing-Hui SHI, Jia-Sheng HAO, Lan-Lan ZHANG, Qun YANG* (E109)

Differentiation in cranial variables among six species of *Hylopetes* (Sciurinae:Pteromyini)

.....*Song LI, Fa-Hong YU* (E120)

Three-dimensional morphology of the *Sinocyclocheilus hyalinus* (Cypriniformes: Cyprinidae) horn based on synchrotron

X-ray microtomography

.....*You HE, Xiao-Yong CHEN, Ti-Qao XIAO, Jun-Xing YANG* (E128)

Effects of Zn²⁺ and Cu²⁺ on loach ovaries and ova development

.....*Jian-Xun TANG, Jun-Rong LI, Zhong-Liang LIU, Hua ZHAO, Xiao-Min TAO, Zhang-Shun CHENG* (E135)

Description of a new *Pratylenchus* species from China (Tylenchida, Pratylenchidae)

.....*Ning LIU, Xiao-Song ZHOU, Li-Jie CHEN, Yu-Xi DUAN* (E140)

The first mitochondrial genome for the butterfly family Riodinidae (*Abisara fylloides*) and its systematic implications

Fang ZHAO¹, Dun-Yuan HUANG^{1,2}, Xiao-Yan SUN³, Qing-Hui SHI¹, Jia-Sheng HAO^{1,*}, Lan-Lan ZHANG¹, Qun YANG^{3,*}

1. College of Life Sciences, Anhui Normal University, Wuhu 24100, China

2. College of Forestry, Jiangxi Environmental Engineering Vocational College, Ganzhou 34100, China

3. Nanjing Institute of Geology and Palaeontology, Chinese Academy of Sciences, Nanjing 21008, China

Abstract: The Riodinidae is one of the lepidopteran butterfly families. This study describes the complete mitochondrial genome of the butterfly species *Abisara fylloides*, the first mitochondrial genome of the Riodinidae family. The results show that the entire mitochondrial genome of *A. fylloides* is 15 301 bp in length, and contains 13 protein-coding genes, 2 ribosomal RNA genes, 22 transfer RNA genes and a 423 bp A+T-rich region. The gene content, orientation and order are identical to the majority of other lepidopteran insects. Phylogenetic reconstruction was conducted using the concatenated 13 protein-coding gene (PCG) sequences of 19 available butterfly species covering all the five butterfly families (Papilionidae, Nymphalidae, Pieridae, Lycaenidae and Riodinidae). Both maximum likelihood and Bayesian inference analyses highly supported the monophyly of Lycaenidae+Riodinidae, which was standing as the sister of Nymphalidae. In addition, we propose that the riordinids be categorized into the family Lycaenidae as a subfamilial taxon.

Keywords: *Abisara fylloides*; Mitochondrial genome; Riodinidae; Systematic implication

The typical metazoan mitochondrial genome (mitogenome) contains 37 genes, including 13 protein-coding genes (PCGs), 2 rRNA genes and 22 tRNA genes, and a non-coding area (i.e., the control region or the A+T-rich region) (Wolstenholme, 1992; Boore, 1999). Maternal inheritance, lack of recombination and an accelerated evolutionary rate compared with the nuclear genome have all contributed to the increased use of mitogenomes, which is one of the key methods in fields such as phylogenetics, comparative and evolutionary genomics, molecular evolution and population genetics (Ballard & Whitlock, 2004; Simonsen et al, 2006). At present, mitochondrial genomes have already been determined in a variety of insect groups covering nearly 200 species. However, reported complete mitogenomes are relatively scarce for lepidopterans and especially for butterflies. To our knowledge, as of October 2012 only about 20 butterfly species covering five butterfly families (Table 2) have been reported or deposited into the GenBank, but only one butterfly family, the Riodinidae, still lack corresponding data.

The phylogenetic position and taxonomic ranking of

the butterfly family Riodinidae among butterfly lineages are still controversial issues among entomologists. Some scholars suggest that the riordinids are closely related to the lycaenids, considering the similarities in morphological character, behavior, and host plants between the two (slug-like larvae, pupa *contigua*, ants associated) (Ackery, 1984; Chou, 1998; de Jong et al, 1996; Ehrlich, 1958; Scott, 1985). Moreover, they are usually classified into the Lycaenidae family as a subfamilial taxon. Some consider the riordinids a unique family parallel to the Lycaenidae

Received: 27 November 2012; Accepted: 06 May 2013

Foundation items: This work was supported by the National Natural Science Foundation of China (41172004), Provincial Key Projects of the Natural Science Foundation in the Colleges of Anhui province (KJ2010A142), Opening Funds from the State Key Laboratory of Palaeobiology and Stratigraphy, Nanjing Institute of Geology and Palaeontology, Chinese Academy of Sciences (104143) and the Program for Innovative Research Teams in Anhui Normal University.

* Corresponding author, E-mail: jshaonigpas@sina.com

family (Campbell et al, 2000; de Jong et al, 1996; Kristensen, 1976; Shou et al, 2006), and others propose that the riordinids are more closely related to the nymphalids than to the other butterfly groups, such as the lycaenids (Martin & Pashley, 1992; Robbins, 1987, 1988).

This study sequenced the first complete mitochondrial genome of the *Abisara fylloides*, a representative species of the family Riordinidae, by long PCR and primer walking techniques. Its genetic structure was preliminarily compared with those of other available butterfly species. The maximum likelihood (ML) and Bayesian inference (BI) phylogenetic trees of the *A. fylloides* and other available butterfly representative species were reconstructed based on concatenated DNA sequences of the 13 protein-coding genes (PCGs), and aim to clarify their phylogenetic relationships and further provide new information about the structure, organization and molecular evolution of the lepidopteran mitogenomes.

MATERIALS AND METHODS

Sample collection and DNA extraction

Adult individuals of *A. fylloides* were collected in

Jinghong, Yunnan Province, China in August 2006. After collection, sample specimens were preserved in 100% ethanol immediately and stored at -20 °C before DNA extraction (specimen No. ZHF07). Total Genomic DNA was isolated using the proteinase K-SiO₂ method as described by Hao et al (2005).

PCR amplification and sequence determining

The multiple sequence alignments were conducted using the software Clustal X 1.8 based on the mitogenome sequences of *Coreana raphaelis*, *Artogeia melete*, *Troides aeacus* available from GenBank and those of *Argyreus hyperbius*, *Acraea issoria*, *Calinaga davidis*, *Pieris rapae* determined in our laboratory (Thompson et al, 1997). The long PCR primers, which may cover the whole mitogenome, were designed according to the conserved regions by the software Primer premier 5.0 (Singh et al, 1998) (Table 1). Seven short fragment sequences (500-700 bp) of cox1, cox2, cox3, cytb, nad1, rrnL and rrnS were amplified using insect universal primers (Caterino & Sperling, 1999; Simmons & Weller, 2001; Simon et al, 1994). All the primers were synthesized by the Shanghai Sheng gong Biotechnology Co. Ltd.

Table 1 List of PCR primers used in this study

Genes	Forward primers (5')	Reverse primers (3')	Annealing temperature (°C)
cox1*	GGTCAACAAATCATAAAGATATTG	TAAACTTCAGGGTGACCAAAAAT	50.0
cox1-cox2	TTATTGTATGAGCCGTAG	ATAGCAGG AAGATTGTTTC	47.5
cox2*	GAGACCATTACTTGCTTCAGTCACT	CTAATATGGCAGATTATATGTATGG	49.5
cox2-cox3	TTTTATTGCTCTTCATCT	TTATTCTCATCGTAATCC	48.5
cox3*	TATTCATGATGACGAGAT	CAAATCCAAATGGTGAGT	49.8
cox3-nad5	TTTATAGCAACAGGATTTC	CATCAACTGGTTAACCTT	45.5
nad5	AAAACCTCCAGAAAATAATCTC	TTGCTTATCTACTTTAACAGACA	46.5
nad5-cytb	AATTATACCAAGCACATAT	TTATCGACTGCAAATC	47.1
cytb*	TATGTACTACCATGAGGACAAATAT	ATTACACCTCTTAATTATTAGGAAT	47.0
cytb-nad1	TCC TGCTAACCTTTAGTC	AGGTAGATTACGGCTGTT	48.0
nad1*	CGTAAAGTCCTAGGTTATTCAGATCG	ATCAAAAGGAGCTCGATTAGTTTC	52.0
nad1-rrnL	AGCCCGTAATCTACCTAA	TAAGACCGAGAAGACCCCTAT	47.0
rrnL*	CGCCTGTTATCAAAACAT	CCGGTCTGAACTCAGAT	45.5
rrnL-rrnS	AGACTATTGATTATGCTACCT	TAAGAATCTAATGGATTACAA	46.5
rrnS*	CTTCTACTTTGTTACGACTTAT	AATTTTGCCAGCAGTTG	50.0
rrnS-nad2	AGAGGGTATCTAATCCGAGTTT	TGGCTGAGAATTAAGCGATA	49.5
nad2-cox1	ATACAGAAGCAGCATTAA	AGAAGGAGGAAGAAGTCAA	52.0

*: universal primer.

Seven partial gene sequences were initially sequenced under the following conditions: an initial denaturation at 94 °C for 5 minutes, then denaturation at 94 °C for 1 minute for a total of 35 cycles; annealing at 45–55 °C for 1 minute and extension at 72 °C for 2 minutes plus 30 seconds; final extension at 72 °C for 10 minutes. Long PCRs were performed using TaKaRa LA

Taq polymerase with the following cycling parameters: an initial denaturation for 5 minutes at 95 °C; followed by 30 cycles at 95 °C for 55 seconds, 45–55 °C for 2 minutes, 68 °C for 2 min and 30 seconds; and a subsequent final extension step of 68 °C for 10 minutes.

The PCR products were separated by electrophoresis in a 1.2% agarose gel and purified using the DNA gel

extraction kit (TaKaRa). All PCR fragments were sequenced directly after purification with the QIA quick PCR Purification Kit reagents (QIAGEN). Internal primers were applied to complete sequences by primer walking (detailed primer information will be provided upon request). All fragments were sequenced for both strands.

Data analysis

We used DNASIS MAX (Hitachi) for sequence assembly and annotation. Protein-coding genes and rRNA genes were identified by sequence comparison with other available insect mitochondrial sequences. The tRNAs were identified by tRNAscan-SE v.1.21 (Lowe & Eddy, 1997). The putative tRNAs, which were not found by tRNAscan-SE, were identified by a sequence comparison of *A. fylloides* with the other lepidopteran tRNAs. PCGs were aligned with the other available lepidopteran mitogenomes using DAMBE software (Xia & Xie, 2001). The tandem repeats in the A+T-rich region were predicted using the Tandem Repeats Finder online (<http://tandem.bu.edu/trf/trf.html>) (Benson, 1999). Nucleotide composition was calculated using PAUP 4.0b10 (Swofford, 2002). The mitogenome sequence data have been deposited in GenBank under the accession number HQ259069.

Phylogenetic analysis

Phylogenetic analyses were performed on 19 representative species including *A. fylloides*, covering all the six families of butterflies. The multiple aligning of the concatenated nucleotide sequences of the 13 mitochondrial PCGs of the 19 species (Table 2) was conducted using ClustalX 1.8. The phylogenetic trees were reconstructed with the maximum likelihood (ML) and Bayesian inference (BI) methods, using the moth species *Adoxophyes honmai* (GenBank accession number of mitogenome: NC014295) as the outgroup. In both phylogenetic analyses, the third codon position of all the sequences was excluded. The ML analyses were conducted in PAUP 4.0b10 by using TBR branch swapping (10 random addition sequences) as a search method. The model GTR+I+Γ was selected as the best fit model using Modeltest 3.06 (Posada & Crandall, 1998) under the AIC scores, and the bootstrap values of the ML tree were evaluated via the bootstrap test with 1 000 iterations. The Bayesian analysis was performed using MrBayes 3.1.2 (Huelsenbeck & Ronquist, 2001) with the partitioned strategy (13 partitions: cox1, cox2, cox3, atp8, atp6, nad1, nad2, nad4, nad4L, nad5, nad6 and cytb), and the best substitution model for each partition was selected as in the ML analysis. The MCMC analyses (with random starting trees) were run with one cold and three heated chains simultaneously for 1,000,000 generations sampled every 100 generations with a burn-in of 25% until the average standard deviation of split

frequencies to be less than 0.01, which means that convergence was reached.

RESULTS AND DISCUSSION

Genome structure and organization

The complete mitogenome is 15 301 bp in length, encodes 37 genes in all. It contains 13 protein, 22 tRNA, 2 rRNA genes and a non-coding high A+T content region (Figure 1, Table 3). Its structure and organization are identical to those of the majority of other lepidopterans (Bae et al, 2004; Cha et al, 2007; Cameron & Whiting, 2008; Hao et al, 2012; Hong et al, 2008, 2009; Hu et al, 2010; Kim et al, 2009b; Ji et al, 2012; Junqueira et al, 2004; Wang et al, 2011), though a few lepidopterans, such as three *Thitarodes* species, were reported to possess the ancestral gene order trnI-trnQ-trnM instead of the trnM-trnI-trnQ (Cao et al, 2012).

Eight overlapping sequences totaling 61 bp are located throughout the *A. fylloides* mitogenome, with size ranging from 2 to 35 bp, of which the longest (35 bp) is located between the cox2 and the tRNA^{Lys} genes. In addition, 17 intergenic spacers ranging from 1 to 45 bp in length are found in the mitogenome. Among these spacers, the longest is located between the tRNA^{Gln} and nad2 genes, the other 16 spacers are scattered throughout the whole genome (Figure 1, Table 3). Most of these spacer regions are arranged relatively compactly

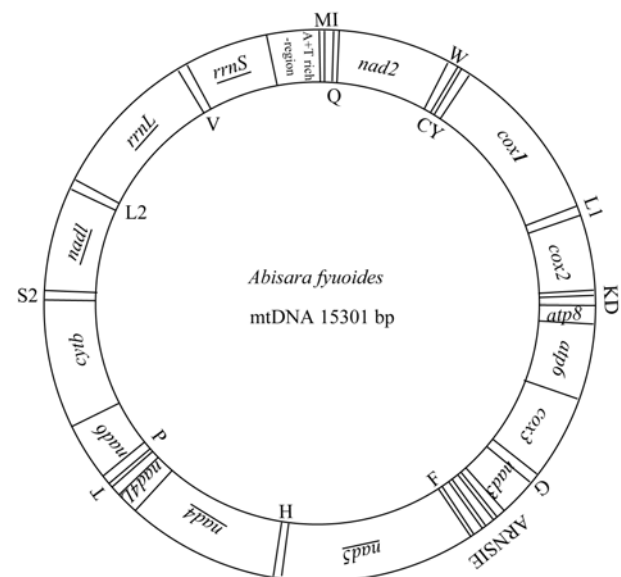


Figure 1 Circular map of the mitochondrial genome of *Abisara fylloides*

Gene names not underlined indicate the direction of transcription from left to right and those underlined indicate right to left. Transfer RNA genes encoded by H and L strands are shown outside and inside the circular gene map, respectively. Transfer RNA genes are indicated by the IUPAC-IUB single letter amino acid codes, while L1, L2, S1, S2 represent tRNA-Leu(UUR), tRNA-Leu(CUN), tRNA-Ser(AGN) and tRNA-Ser(UCN), respectively.

Table 2 The available rhopaloceran mitogenomes and their characteristics

Family	Subfamily	Species	Whole genome		PCG ^b	rml	rrnS	AT-rich region	GenBank accession no.	References
			Size (bp)	(A+T) %						
Papilionidae	Papilioninae	<i>Teinopalpus aureus</i>	15 242	79.8	3 720	78.3	1 320	82.4	781	85.6
		<i>Papilio machaon</i>	15 185	80.3	3 707	79.0	1 319	83.5	773	84.2
Parnassiidae	Parnassiinae	<i>Parnassius bremeri</i>	15 389	81.3	3 723	80.2	1 344	83.9	773	85.1
		<i>Ctenophilum vasava</i>	15 468	80.5	3 698	78.9	1 343	84.1	774	86.4
Hesperiidae	Pyrginae	<i>Parnara guttata</i>	15 411	80.6	3 718	78.9	1 368	84.5	778	85.1
	Hesperiinae	<i>Choaspes benjamini</i>	15 272	80.8	3 681	79.0	1 355	85.2	777	86.0
Pieridae	Pierinae	<i>Artogeia melete</i>	15 140	79.8	3 715	78.4	1 319	83.4	777	85.5
		<i>Pieris rapae</i>	15 157	79.7	3 722	78.3	1 320	84.0	764	85.0
Lycaenidae	Theclinae	<i>Coreana raphaelis</i>	15 314	82.7	3 708	81.5	1 330	85.3	777	85.8
		<i>Protanitis superans</i>	15 248	81.7	3 712	80.3	1 331	85.1	739	85.6
Aphnaeinae	Spindasis takanonis	<i>Spindasis takanonis</i>	15 349	82.4	3 719	81.0	1 333	85.6	777	84.7
	Apaturinae	<i>Apatura ilia</i>	15 242	80.5	3 711	78.9	1 333	84.0	776	84.9
Nymphalidae	Sasakia charonda	<i>Sasakia charonda</i>	15 244	79.9	3 695	78.2	1 323	84.4	775	85.0
	Kallima inachus	<i>Kallima inachus</i>	15 183	80.3	3 721	79.2	1 335	82.7	774	85.1
Heliconiidae	Argyreus hyperbius	<i>Argyreus hyperbius</i>	15 156	80.8	3 718	79.5	1 330	84.5	778	85.2
	Acrea issoria	<i>Acrea issoria</i>	15 245	79.7	3 717	78.0	1 331	83.9	788	83.7
Limenitidinae	Athyra subpitia	<i>Athyra subpitia</i>	15 268	81.9	3 729	80.6	1 319	84.7	779	85.7
	Libytheinae	<i>Libythea celtis</i>	15 164	81.2	3 722	80.0	1 335	84.7	775	85.4
Riodinidae	Nemeobiinae	<i>Abisara fyllodes</i>	15 301	81.2	3 730	79.8	1 334	85.4	771	85.6

a: Termination codons were excluded in total codon count. b: Protein-coding genes.

Table 3 Organization of the *Abisara fylloides* mitochondrial genome

Gene	Direction	Position	Size (bp)	Intergenic length*	Start codon	Stop codon
tRNA ^{Met}	F	1–67	67	0		
tRNA ^{Ile}	F	68–131	64	-3		
tRNA ^{Gln}	R	129–197	69	45		
nad2	F	243–1 256	1 014	1	ATT	TAA
tRNA ^{Trp}	F	1 258–1 324	67	-8		
tRNA ^{Cys}	R	1 317–1 382	66	3		
tRNA ^{Tyr}	R	1 386–1 451	66	6		
cox1	F	1 458–2 989	1 532	3	CGA	T
tRNA ^{Leu(UUR)}	F	2 993–3 059	67	0		
cox2	F	3 060–3 738	679	-3	ATG	T
tRNA ^{Lys}	F	3 736–3 806	71	0		
tRNA ^{Asp}	F	3 807–3 871	65	0		
atp8	F	3 872–4 033	162	-7	ATC	TAA
atp6	F	4 027–4 714	688	-2	ATG	TAA
cox3	F	4 713–5 501	789	2	ATG	TAA
tRNA ^{Gly}	F	5 504–5 569	66	0		
nad3	F	5 570–5 923	354	3	ATT	TAA
tRNA ^{Ala}	F	5 927–5 997	71	3		
tRNA ^{Arg}	F	6 001–6 064	64	1		
tRNA ^{Asn}	F	6 066–6 131	66	16		
tRNA ^{Ser(AGN)}	F	6 148–6 208	61	1		
tRNA ^{Glu}	F	6 210–6 275	66	-2		
tRNA ^{Phe}	R	6 274–6 340	67	0		
nad5	R	6 341–8 108	1 768	0	ATT	T
tRNA ^{His}	R	8 109–8 179	71	6		
nad4	R	8 186–9 518	1 333	-2	ATG	T
nad4L	R	9 517–9 805	289	2	ATG	TAA
tRNA ^{Thr}	F	9 808–9 870	63	0		
tRNA ^{Pro}	R	9 871–9 937	67	5		
nad6	F	9 943–10 467	525	3	ATA	TAA
cytb	F	10 471–11 622	1 152	-2	ATG	TAA
tRNA ^{Ser(UCN)}	F	11 621–11 685	65	17		
nad1	R	11 703–12 641	939	1	ATG	TAA
tRNA ^{Leu(CUN)}	R	12 643–12 710	68	0		
rrnL	R	12 711–14 044	1 334	0		
tRNA ^{Val}	R	14 045–14 107	63	0		
rrnS	R	14 108–14 878	771	0		
A+T-rich region		14 879–15 301	423			

*: In the column intergenic length, the positive number indicates interval base pairs between genes, while the negative number indicates the overlapping base pairs between genes.

compared with other insect mitogenomes (Cameron & Whiting, 2008; Hao et al, 2012; Hong et al, 2009; Hu et al, 2010; Kim et al, 2009b; Ji et al, 2012; Junqueira et al, 2004; Wang et al, 2011).

The *A. fylloides* A+T-rich region is flanked on one side by the rrnS and on the other side by the tRNA^{Met} genes. This region exhibits the highest A+T content (91.0%) (Table 4), and spans 423 bp (Table 3, Table 4). A sequence analysis of the A+T-rich region revealed that it contained some structures typical of other lepidopteran mitogenomes: (1) at 20 bp downstream of the small subunit rRNA gene, there is a structure including a motif ‘ATAGA’ which is very well conserved in all sequenced lepidopteran insects, and a 18-bp polyT

stretch, both of which have been suggested as the origin of minority or light strand replication (O_N) and to play a regulatory role (Kim et al, 2009a; Lutz-Bonengel et al, 2004; Saitou et al, 2005; Yukihiro et al, 2002). (2) Between the sites 15 151 and 15 168 there is a microsatellite-like (TA)₉ element, which is also found in the majority of other lepidopterans; (3) There is another motif “ATTAA” of unknown function located from 15 139 to 15 143 upstream of the (TA)₉, which is also typical of the other lepidopterans. In addition, to our great surprise, an unexpected short microsatellite-like repeating region (TA)₁₁ downstream of the (TA)₉ was detected in the A+T-rich region, and this has not been reported in any other lepidopterans.

Table 4 Nucleotide composition and skewness in different regions of the *Abisara fylloides* mitogenome

Region	Size (bp)	Nucleotide composition (%)					AT-skew	GC-skew
		T	C	A	G	A+T		
Whole genome	15 301	41.7	11.3	39.5	7.5	81.2	-0.027	-0.202
Major-strand PCGs	6 927	44.5	12.1	34.1	9.3	78.6	-0.132	-0.131
Minor-strand PCGs	4 329	47.6	6.3	34.1	12.0	81.7	-0.165	0.311
Whole PCGs	11 224	45.8	9.9	34.0	10.3	79.8	-0.148	0.020
Whole tRNA	1 461	40.0	7.7	41.5	10.7	81.5	0.018	0.163
rrnL	1 334	38.4	4.8	47.0	9.8	85.4	0.101	0.342
rrnS	771	39.9	4.9	45.7	9.5	85.6	0.068	0.319
A+T-rich region	423	48.9	4.5	42.1	4.5	91.0	-0.075	0.000

Base composition bias

The base composition of the *A. fylloides* mitogenome shows an A and T bias (Table 4). The whole A+T content of the mitogenome is up to 81.2%, ranging from that of *Argyreus hyperbius* (80.81%) to that of *Coreana raphaelis* (82.66%). Like most other metazoan mitogenomes, the A+T content of the A+T-rich region, which is located between the rrnS and tRNA^{Met} genes, is the highest (91.0%) in all known butterfly species except for *P. rapae* (Pieridae) to date. The base contents of A, T, C, G are 39.5%, 41.7%, 11.3%, 7.5%, respectively, indicating a relatively higher A+T content (81.2%). These phenomena commonly exist in the protein-coding genes, which have a relatively lower A+T content (79.8%), and the tRNA and rRNA genes in insects.

Protein-coding genes

The sequences of the 13 *Abisara fylloides* PCGs are 11 224 bp in length, including 3 730 codons (excluding termination codons). Twelve of the 13 PCGs use standard ATN as their start codon except for the cox1 gene, and eight of these 12 PCGs begin with ATA or ATG (Methionine) and the other four begin with ATT or ATC (Isoleucine) (Table 3). The start codons for cox1 gene of lepidopteran insects have usually been a controversial issue. In general, there is no typical start codon, especially for the cox1 gene, which usually uses CAG (R) as start codon in insects, including the lepidopterans. However, some scholars reported unusual start codons, such as the trinucleotide TTG (Bae et al, 2004; Hong et al, 2008), ACG (Lutz-Bonengel et al, 2004), GCG (Nardi et al, 2003), the tetranucleotide ATAA, ATCA and ATTA (Clary & Wolstenholme, 1983; de Bruijn, 1983; Kim et al, 2006), and the hexanucleotides TATTAG (Flook et al, 1995), TTTTAG (Yukihiro et al, 2002), TATCTA (Coates et al, 2005), ATTAA (Beard et al, 1993; Mitchell et al, 1993) for cox1 in some other insect species. However, the CGA is present as a conserved region for all lepidopteran insects reported, and thus

we tend to consider that CGA is the cox1 start codon for *A. fylloides* as Kim et al (2009b) suggested. As for stop codons, 9 of the 13 PCGs use standard TAA except for the cox1, cox2, nad4 and nad5 genes, all of which terminate at a single thymine (Table 3), and this case was also found in all other lepidopterans reported to date. For more details on this phenomenon, please refer to the discussions of Kim et al. (2010).

The PCG amino acid sequence variation analysis showed that there were 3 755 homologous sites, of which 1 964 are conserved, 1 791 are variable, and 1 128 are parsimony informative. Among the twenty amino acids in the 13 PCGs, six (Leu, Met, Ile, Phe, Asn, and Tyr) were used more frequently than the others, and their usage frequencies were higher than the average, whereas the other 14 amino acids less used (Table 5).

rRNA and tRNA genes

The large subunit rRNA and small subunit rRNA genes of the *A. fylloides* are 1 334 and 771 bp in length, respectively. As in other lepidopterans, these two genes are located between tRNA^{Leu(UUR)} and tRNA^{Val}, and between tRNA^{Val} and A+T-rich region respectively (Cameron & Whiting, 2008; Hao et al, 2012; Hu et al, 2010; Kim et al, 2009a; Salvato et al, 2008; Wang et al, 2011; Yang et al, 2009).

The *A. fylloides* mitogenome harbors 22 tRNA genes, which are scattered throughout the whole genome and ranged in length from 61 to 71 bp. Except for the tRNA^{Ser(AGN)}, which lacks the DHU loop, all tRNAs are shown to be folded into the cloverleaf secondary structures, within which all amino acid acceptor stems have 7 base pairs, and all anticodon stems have 5 base pairs. This was also found in all the other lepidopterans determined to date (Cameron & Whiting, 2008; Hao et al, 2012; Hu et al, 2010; Kim et al, 2009a).

A total of 27 pairs of base mismatches were detected in all the predicted tRNA secondary structures, among which 17 are GU, 6 are UU, 2 are AA, and 2 are AC. The AA mismatches occur at the anticodon stem of

Table 5 Codon usage of the protein-coding genes of the *Abisara fylloides* mitogenomes

Codon	N (RSCU)						
UUU (F)	356 (1.86)	UCU (S)	108 (2.59)	UAU (Y)	175 (1.83)	UGU (C)	28 (1.81)
UUC (F)	26 (0.14)	UCC (S)	16 (0.38)	UAC (Y)	16 (0.17)	UGC (C)	3 (0.19)
UUA (L)	488 (5.30)	UCA (S)	94 (2.25)	UAA (*)	0 (0)	UGA (W)	84 (1.87)
UUG (L)	12 (0.13)	UCG (S)	2 (0.05)	UAG (*)	0 (0)	UGG (W)	6 (0.13)
CUU (L)	34 (0.37)	CCU (P)	70 (2.33)	CAU (H)	62 (1.85)	CGU (R)	14 (1.04)
CUC (L)	3 (0.03)	CCC (P)	9 (0.3)	CAC (H)	5 (0.15)	CGC (R)	0 (0)
CUA (L)	14 (0.15)	CCA (P)	38 (1.27)	CAA (Q)	57 (1.93)	CGA (R)	37 (2.74)
CUG (L)	1 (0.01)	CCG (P)	3 (0.1)	CAG (Q)	2 (0.07)	CGG (R)	3 (0.22)
AUU (I)	424 (1.88)	ACU (T)	74 (2.1)	AAU (N)	251 (1.81)	AGU (S)	25 (0.6)
AUC (I)	27 (0.12)	ACC (T)	7 (0.2)	AAC (N)	26 (0.19)	AGC (S)	0 (0)
AUA (M)	283 (1.81)	ACA (T)	59 (1.67)	AAA (K)	97 (1.92)	AGA (S)	89 (2.13)
AUG (M)	29 (0.19)	ACG (T)	1 (0.03)	AAG (K)	4 (0.08)	AGG (S)	0 (0)
GUU (V)	74 (2.39)	GCU (A)	73 (2.52)	GAU (D)	55 (1.83)	GGU (G)	56 (1.17)
GUC (V)	4 (0.13)	GCC (A)	8 (0.28)	GAC (D)	5 (0.17)	GGC (G)	1 (0.02)
GUA (V)	45 (1.45)	GCA (A)	33 (1.14)	GAA (E)	65 (1.78)	GGA (G)	100 (2.08)
GUG (V)	1 (0.03)	GCG (A)	2 (0.07)	GAG (E)	8 (0.22)	GGG (G)	35 (0.73)

n: frequency of codon used; RSCU: relative synonymous codon usage; *:stop codon.

Stop codons were excluded in total codon counts.

tRNA^{Lys} and the TψC loop of tRNA^{Trp}; the AC mismatches occur at the amino acid acceptor stem of tRNA^{Tyr} and the anti codon stem of tRNA^{Leu(UUR)}. Among the 6 UU mismatches, two occur at the amino acid acceptor stems of tRNA^{Leu(UUR)} and tRNA^{Ala}, two at the anti codon stems of tRNA^{Leu(UUR)} and tRNA^{Gln}, and another two at the anti codon stem of tRNA^{Ser(UCN)}, respectively (Figure 2).

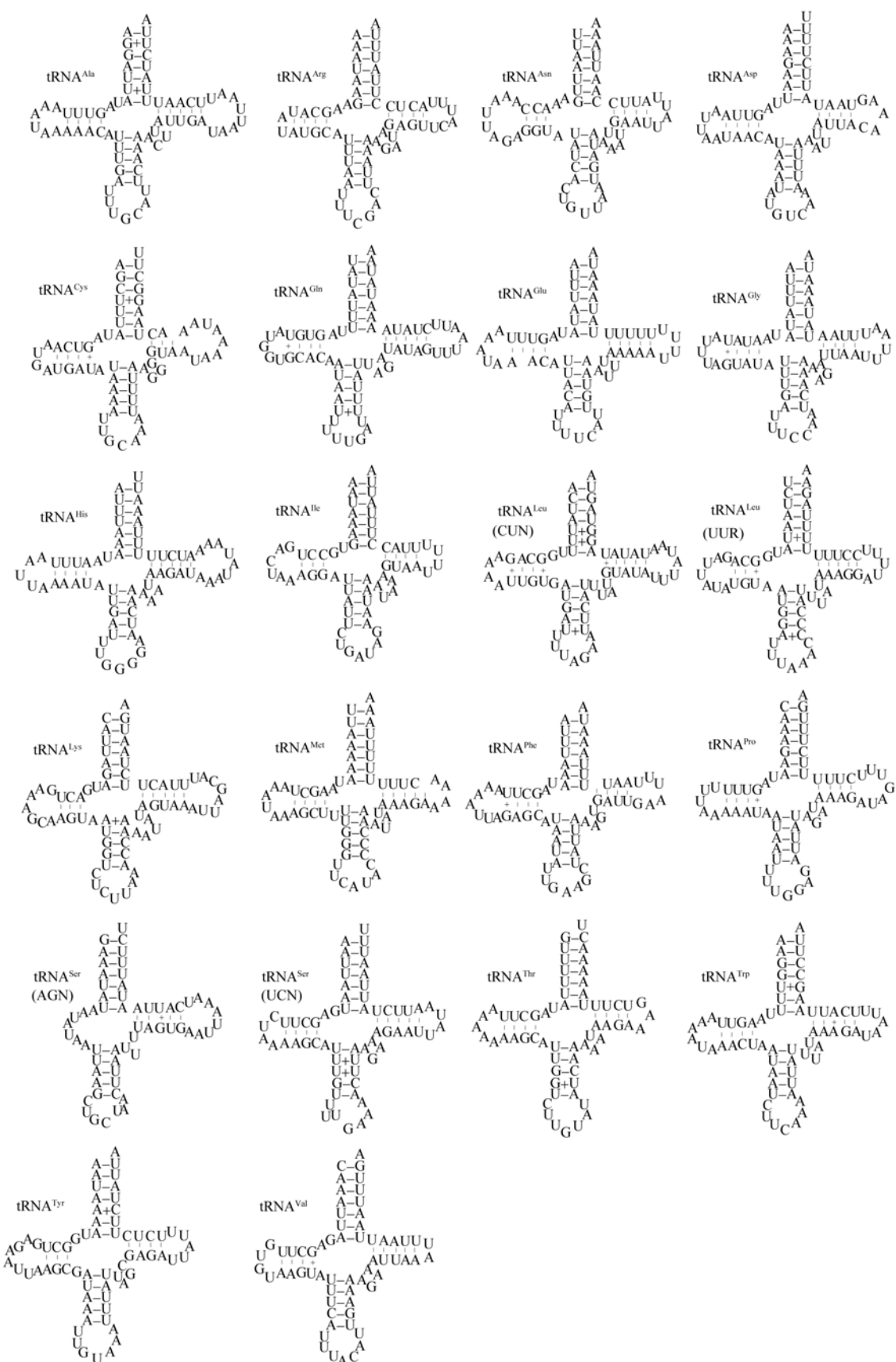
Phylogenetic analysis

At present, for the phylogenetic positions of the riodinids within papilionid butterflies, most morphological studies place them as most closely related to the lycaenids and identify the nymphalids as the closest relatives to this riodinid+lycaenid clade (de Jong et al, 1996; Ehrlich & Ehrlich, 1967; Kristensen, 1976; Scott & Wright, 1990). These relationships have been inferred using a variety of phylogenetic methods and are supported by a number of adult, larval and pupal synapomorphies. Additionally, molecular (DNA sequence of the mitochondrial NADH1 gene) or molecular plus morphological evidence also result in a monophyletic interpretation of the Riodinidae+Lycaenidae, and their sister relationship to the Nymphalidae (Wahlberg et al, 2005; Weller et al, 1996). However, based on a cladistic analysis of four foreleg characters with nine character states, Robbins (1988) suggested that the Riodinidae are more closely related to the Nymphalidae than to the Lycaenidae, and this result is supported by the nuclear 28S rRNA gene sequence data (Martin & Pashley, 1992).

There are two opinions regarding the taxonomic rank of riodinids. First, some previous studies suggest

that the riodinids should be categorized into the family lycaenids as a subfamilial taxon in light of their morphological characters (Chou, 1998; de Jong et al, 1996; Ehrlich, 1958; Kristensen, 1976; Scott & Wright, 1990), and this opinion is supported by the molecular studies of Zou et al (2009) and Hao et al (2007). Other studies postulate that the riodinids should be classified as a separate family parallel to Lycaenidae (Harvey, 1987; Martin & Pashley, 1992; Robbins, 1988; Weller et al, 1996), and this view is supported by molecular phylogenetic studies based on data from the wingless gene by Campbell et al (2000) and the combined analysis of sequences of the nuclear Ef-1a, wingless, and mitochondrial COI genes by Wahlberg et al (2005).

The ML and Bayesian trees of this study (Figure 3) showed that all the butterfly taxa in this study did not form a monophyletic unit, and a similar case was reported by Hao et al (2012). Nonetheless, both the ML and BI trees indicated that all the butterfly species were grouped into five distinct lineages: 1) the Papilionidae, including papilionids and parnassids; 2) Hesperiidae; 3) Pieridae; 4) Nymphalidae; 5) Lycaenidae+Riodinidae. The monophyly of Lycanidae + Riodinidae was strongly supported with a 100% bootstrap value in ML, and with 1.00 posterior probability value in BI. Thus, considering the results of Heikkilä et al (2012), which indicate the monophlyies of lycaenids and riodinids, it is reasonable to propose that the two groups may be sisters, though the taxa sampling of riodinids in this analysis is extremely limited. Additionally, based their congruent genetic divergences compared with those between other butterfly subfamilies, the riodinids should be categorized into the Lycaenidae family as a subfamilial taxon.

Figure 2 Predicated clover-leaf secondary structures for the mitochondrial tRNA genes of *Abisara fylloides*

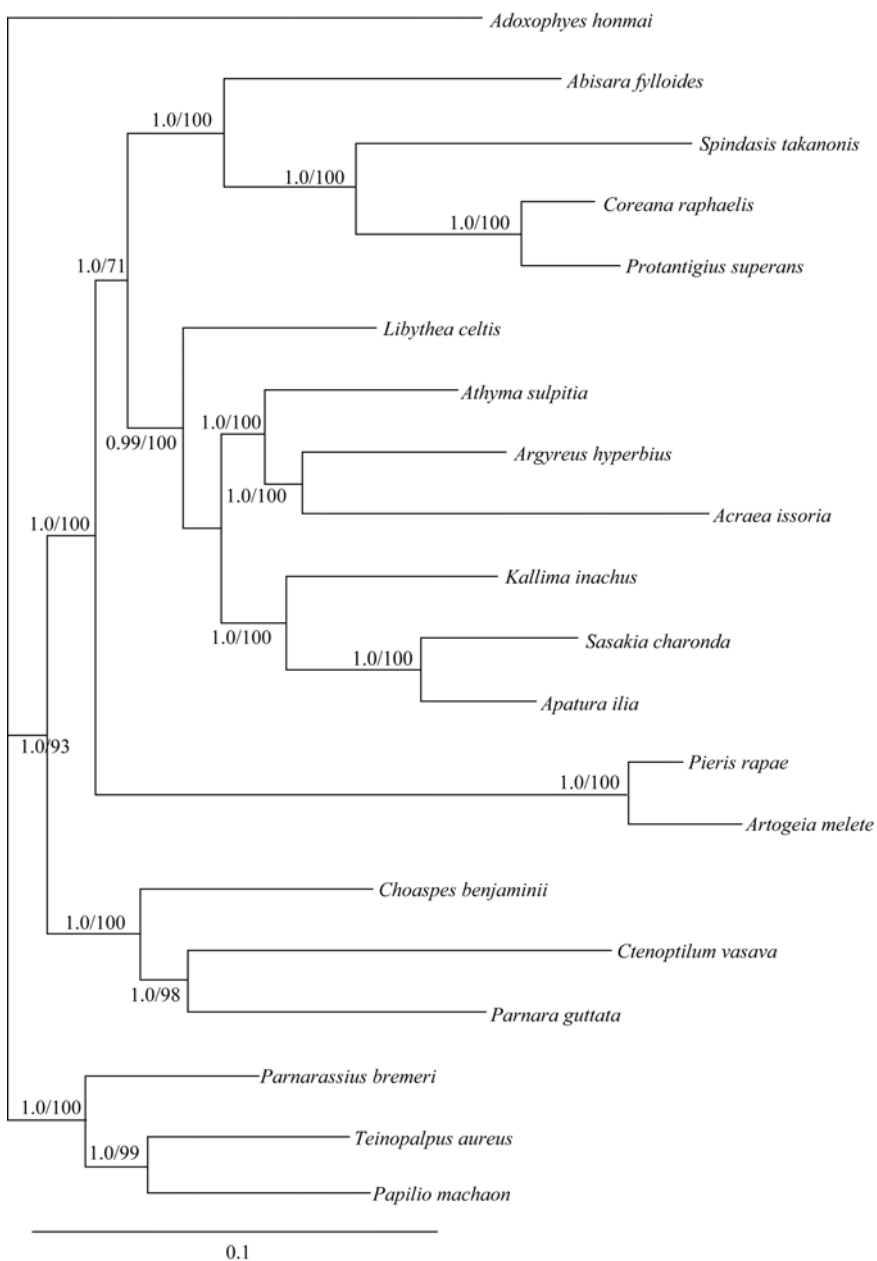


Figure 3 The Bayesian inference (BI) and maximum likelihood (ML) phylogenetic trees of main butterfly lineages based on 13 protein-coding gene sequences (Numbers on each node correspond to the posterior probability values of the BI analysis and the ML bootstrap percentage values for 1 000 replicates of ML analysis)

References

Ackery PR. 1984. Systematic and faunistic studies on butterflies. In: Vane-Wright RI, Ackery PR. The Biology of Butterflies. London: Academic Press.

Bae JS, Kim I, Sohn HD, Jin BR. 2004. The mitochondrial genome of the firefly, *Pyrocoelia rufa*: complete DNA sequence, genome organization, and phylogenetic analysis with other insects. *Molecular Phylogenetics and Evolution*, **32**(3): 978-985.

Ballard JWO, Whitlock MC. 2004. The incomplete natural history of mitochondria. *Molecular Ecology*, **13**(4): 729-744.

Beard CD, Hamm SM, Collins FH. 1993. The mitochondrial genome of the mosquito *Anopheles gambiae*: DNA sequence, genome organization, and comparisons with mitochondrial sequences of other insects. *Insect Molecular Biology*, **2**(2): 103-124.

Benson G. 1999. Tandem repeats finder: a program to analyze DNA sequences. *Nucleic Acids Research*, **27**(2): 573-580.

Boore JL. 1999. Animal mitochondrial genomes. *Nucleic Acids Research*, **27**(8): 1767-1780.

Cao YQ, Ma C, Chen JY, Yang DR. 2012. The complete mitochondrial genomes of two ghost moths, *Thitarodes renzhiensis* and *Thitarodes*

yunnanensis: the ancestral gene arrangement in Lepidoptera. *BMC Genomics*, **13**(1): 276.

Cameron SL, Whiting MF. 2008. The complete mitochondrial genome of the tobacco hornworm, *Manduca sexta*, (Insecta: Lepidoptera: Sphingidae), and an examination of mitochondrial gene variability within butterflies and moths. *Gene*, **408**(1-2): 112-123.

Campbell DL, Brower AVZ, Pierce NE. 2000. Molecular evolution of the wingless gene and its implications for the phylogenetic placement of the butterfly family Riodinidae (Lepidoptera: Papilionoidea). *Molecular Biology and Evolution*, **17**(5): 684-696.

Caterino MS, Sperling FAH. 1999. *Papilio* phylogeny based on mitochondrial cytochrome oxidase I and II genes. *Molecular Phylogenetics and Evolution*, **11**(1): 122-137.

Cha SY, Yoon HJ, Lee EM, Yoon MH, Hwang JS, Jin BR, Han YS, Kim I. 2007. The complete nucleotide sequence and gene organization of the mitochondrial genome of the bumblebee, *Bombus ignitus* (Hymenoptera: Apidae). *Gene*, **392**(1-2): 206-220.

Chen M, Tian LL, Shi QH, Cao TW, Hao JS. 2012. Complete mitogenome of the Lesser Purple Emperor *Apatura ilia* (Lepidoptera: Nymphalidae: Apaturinae) and comparison with other nymphalid butterflies. *Zoological Research*, **33**(2): 191-201.

Chou I. 1998. Classification and Identification of Chinese Butterflies[M]. Zhengzhou: Henan Scientific and Technological Publishing House. (in Chinese)

Coates BS, Sumerford DV, Hellmich RL, Lewis LC. 2005. Partial mitochondrial genome sequences of *Ostrinia nubilalis* and *Ostrinia furnicalis*. *International Journal of Biological Sciences*, **1**: 13-18.

Clary DO, Wolstenholme DR. 1983. Genes for cytochrome c oxidase subunit I, URF2, and three tRNAs in *Drosophila* mitochondrial DNA. *Nucleic Acids Research*, **11**(19): 6859-6872.

De Bruijn MHL. 1983. *Drosophila melanogaster* mitochondrial DNA, a novel organization and genetic code. *Nature*, **304**(5932): 234-241.

De Jong R, Vane-Wright RI, Ackery PR. 1996. The higher classification of butterflies (Lepidoptera): problems and prospects. *Insect Systematics & Evolution*, **27**(1): 65-103.

Ehrlich PR. 1958. The Comparative Morphology, Phylogeny and Higher Classification of the Butterflies (Lepidoptera: Papilionoidea). *University of Kansas Science Bulletin*, **39**(8): 305-370.

Ehrlich PR, Ehrlich AH. 1967. The phenetic relationships of the butterflies. I. Adult taxonomy and the nonspecificity hypothesis. *Systematic Biology*, **16**(4): 301-317.

Flook PK, Rowell CH, Gellissen G. 1995. The sequence, organization, and evolution of the *Locusta migratoria* mitochondrial genome. *Journal of Molecular Evolution*, **41**(6): 928-941.

Hao JS, Li CX, Sun XY, Yang Q. 2005. Phylogeny and divergence time estimation of cheilostome bryozoans based on mitochondrial 16S rRNA sequences. *Chinese Science Bulletin*, **50**(12): 1205-1211.

Hao JS, Su CY, Zhu GP, Chen N, Wu DX, Pan HC, Zhang XP. 2007. Mitochondrial 16S rDNA molecular morphology of the main butterflies' lineages and its phylogenetic significance. *Journal of Genetics and Molecular Biology*, **18**(2): 109-121.

Hao JS, Sun QQ, Zhao HB, Sun XY, Gai YH, Yang Q. 2012. The complete mitochondrial genome of *Ctenoptilum vasava* (Lepidoptera: Hesperiidae: Pyrginae) and its phylogenetic implication. *Comparative and Functional Genomics*, **2012**: 328049, doi: 10.1155/2012/328049.

Harvey DJ. 1987. The Higher Classification of the Riodinidae. Ph. D dissertation, University of Texas, Austin.

Heikkilä M, Kaila L, Mutanen M, Peña C, Wahlberg N. 2012. Cretaceous origin and repeated tertiary diversification of the redefined butterflies. *Proceedings of the Royal Society B: Biological Sciences*, **279**(1731): 1093-1099.

Hong GY, Jiang ST, Yu M, Yang Y, Li F, Xue FS, Wei ZJ. 2009. The complete nucleotide sequence of the mitochondrial genome of the cabbage butterfly, *Artogeia melete* (Lepidoptera: Pieridae). *Acta Biochimica et Biophysica Sinica*, **41**(6): 446-455.

Hong MY, Lee EM, Jo YH, Park HC, Kim SR, Hwang JS, Jin BR, Kang PD, Kim KG, Han YS, Kim I. 2008. Complete nucleotide sequence and organization of the mitogenome of the silk moth *Caligula boisduvalii* (Lepidoptera: Saturniidae) and comparison with other lepidopteran insects. *Gene*, **413**(1-2): 49-57.

Hu J, Zhang DX, Hao JS, Huang DY, Cameron S, Zhu CD. 2010. The complete mitochondrial genome of the yellow coaster, *Acraea issoria* (Lepidoptera: Nymphalidae: Heliconiinae: Acraeini): sequence, gene organization and a unique tRNA translocation event. *Molecular Biology Reports*, **37**(7): 3431-3438.

Huelsenbeck JP, Ronquist F. 2001. MRBAYES: Bayesian inference of phylogenetic trees. *Bioinformatics*, **17**(8): 754-755.

Ji LW, Hao JS, Wang Y, Huang DY, Zhao JL, Zhu CD. 2012. The complete mitochondrial genome of the dragon swallowtail, *Sericinus montela* Gray (Lepidoptera: Papilionidae) and its phylogenetic implication. *Acta Entomologica Sinica*, **55**(1): 91-100.

Junqueira ACM, Lessinger AC, Torres TT, da Silva FR, Vettore AL, Arruda P, Espin AMLA. 2004. The mitochondrial genome of the blowfly *Chrysomya chloropyga* (Diptera: Calliphoridae). *Gene*, **339**: 7-15.

Kim I, Lee EM, Seol KY, Yun EY, Lee YB, Hwang JS, Jin BR. 2006. The mitochondrial genome of the Korean hairstreak, *Coreana raphaelis* (Lepidoptera: Lycaenidae). *Insect Molecular Biology*, **15**(2): 217-225.

Kim SR, Kim MI, Hong MY, Kim KY, Kang PD, Hwang JS, Han YS, Jin BR, Kim I. 2009a. The complete mitogenome sequence of the Japanese oak silkworm, *Antheraea yamamai* (Lepidoptera: Saturniidae). *Molecular Biology Reports*, **36**(7): 1871-1880.

Kim MI, Baek JY, Kim MJ, Jeong HC, Kim KG, Bae CH, Han YS, Jin BR, Kim I. 2009b. Complete nucleotide sequence and organization of the mitogenome of the red-spotted apollo butterfly, *Parnassius bremeri* (Lepidoptera: Papilionidae) and comparison with other lepidopteran insects. *Molecules and Cells*, **28**(4): 347-363.

Kim MJ, Wan XL, Kim KJ, Hwang JS, Kim I. 2010. Complete nucleotide sequence and organization of the mitogenome of endangered *Eumenis autonoe* (Lepidoptera: Nymphalidae). *African Journal of Biotechnology*, **9**(5): 735-754.

Kim MJ, Kang RA, Jeong HC, Kim KG, Kim I. 2011. Reconstructing intraordinal relationships in Lepidoptera using mitochondrial genome data with the description of two newly sequenced lycaenids, *Spindasis takanonis* and *Protantigius superans* (Lepidoptera: Lycaenidae). *Molecular Phylogenetics and Evolution*, **61**(2): 436-445.

Kristensen NP. 1976. Remarks on the family-level phylogeny of butterflies (Insecta, Lepidoptera, Rhopalocera). *Journal of Zoological Systematics and Evolutionary Research*, **14**(1): 25-33.

Lowe TM, Eddy SR. 1997. tRNAscan-SE: a program for improved detection of transfer RNA genes in genomic sequence. *Nucleic Acids Research*, **25**(5): 955-964.

Lutz-Bonengel S, Sänger T, Pollak S, Szibor R. 2004. Different methods to determine length heteroplasmy within the mitochondrial control region. *International Journal of Legal Medicine*, **118**(5): 274-281.

Martin JA, Pashley DP. 1992. Molecular systematic analysis of butterfly family and some subfamily relationships (Lepidoptera: Papilionoidea). *Annals of the Entomological Society of America*, **85**(2): 127-139.

Mitchell SE, Cockburn AF, Seawright JA. 1993. The mitochondrial genome of *Anopheles quadrimaculatus* species A: complete nucleotide sequence and gene organization. *Genome*, **36**(6): 1058-1073.

Mao ZH, Hao JS, Zhu GP, Hu J, Si MM, Zhu CD. 2010. Sequencing and analysis of the complete mitochondrial genome of *Pieris rapae* Linnaeus (Lepidoptera: Pieridae). *Acta Entomologica Sinica*, **53**(11): 1295-1304. (in Chinese)

Nardi F, Carapelli A, Dallai R, Frati F. 2003. The mitochondrial genome of the olive fly *Bactrocera oleae*; two haplotypes from distant geographical locations. *Insect Molecular Biology*, **12**(6): 605-611.

Posada D, Crandall KA. 1998. Modeltest: testing the model of DNA substitution. *Bioinformatics*, **14**(9): 817-818.

Qin F, Jiang GF, Zhou SY. 2012a. Complete mitochondrial genome of the *Teinopalpus aureus guangxiensis* (Lepidoptera: Papilionidae) and related phylogenetic analyses. *Mitochondrial DNA*, **23**(2): 123-125.

Qin XM, Guan QX, Zeng DL, Qin F, Li HM. 2012b. Complete mitochondrial genome of *Kallima inachus* (Lepidoptera: Nymphalidae: Nymphalinae): Comparison of *K. inachus* and *Argynnis hyperbius*. *Mitochondrial DNA*, **23**(4): 318-320.

Robbins RK. 1987. Logic and phylogeny: a critique of Scott's phylogenies to the butterflies and Macrolepidoptera. *Journal of the Lepidopterists' Society*, **41**: 214-216.

Robbins RK. 1988. Comparative morphology of the butterfly foreleg coxa and trochanter (Lepidoptera) and its systematic implications. *Proceedings of the Entomological Society of Washington*, **90**: 133-154.

Saitou S, Tamura K, Aotsuka T. 2005. Replication origin of mitochondrial DNA in insects. *Genetics*, **171**(4): 1695-1705.

Salvato P, Simonato M, Battisti A, Negrisolo E. 2008. The complete mitochondrial genome of the bag-shelter moth *Ochrogaster lunifer* (Lepidoptera, Notodontidae). *BMC Genomics*, **9**: 331.

Scott JA. 1985. The phylogeny of butterflies (Papilionoidea and Hesperioidae). *Journal of Research on the Lepidoptera*, **23**(4): 241-281.

Scott JA, Wright DM. 1990. Butterfly phylogeny and fossils // Kudrna O. Butterflies of Europe. Vol 2. Wiesbaden: Aula-Verlag.

Shou JX, Chou I, Li YF. 2006. Systematic Butterfly Names of the World. Xi'an: Shaanxi Science and Technology Press. (in Chinese)

Simmons RB, Weller SJ. 2001. Utility and evolution of cytochrome *b* in insects. *Molecular Phylogenetics and Evolution*, **20**(2): 196-210.

Simon C, Frati F, Bekenbach A, Crespi B, Liu H, Flook P. 1994. Evolution, weighting, and phylogenetic utility of mitochondrial gene sequences and a compilation of conserved polymerase chain reaction primers. *Annals of the Entomological Society of America*, **87**(6): 651-701.

Simonsen TJ, Wahlberg N, Brower AVZ, de Jong R. 2006. Morphology, molecules and fritillaries: approaching a stable phylogeny for Argynnini (Lepidoptera: Nymphalidae). *Insect Systematics and Evolution*, **37**(4): 405-418.

Singh VK, Mangalam AK, Dwivedi S, Naik S. 1998. Primer premier: program for design of degenerate primers from a protein sequence. *Biotechniques*, **24**(2): 318-319.

Swofford DL. 2002. PAUP* 4.0b10: Phylogenetic Analysis Using Parsimony (* and Other Methods), Beta Version. Sunderland: Sinauer Associates.

Thompson JD, Gibson TJ, Plewniak F, Jeanmougin F, Higgins DJ. 1997. The CLUSTALX windows interface: flexible strategies for multiple sequence alignment aided by quality analysis tools. *Nucleic Acids Research*, **25**(24): 4876-4882.

Tian LL, Sun XY, Chen M, Gai YH, Hao JS, Yang Q. 2012. Complete mitochondrial genome of the Five-dot Sergeant *Parathyma sulpitia* (Nymphalidae: Limenitidinae) and its phylogenetic implications. *Zoological Research*, **33**(2): 133-143.

Wahlberg N, Braby MF, Brower AVZ, de Jong R, Lee MM, Nylin S, Pierce N, Sperling FA, Vila R, Warren AD, Zakharov E. 2005. Synergistic effects of combining morphological and molecular data in resolving the phylogeny of butterflies and skippers. *Proceedings of the Royal Society B: Biological Sciences*, **272**(1572): 1577-1586.

Wang XC, Sun XY, Sun QQ, Zhang DX, Hu J, Yang Q, Hao JS. 2011. Complete mitochondrial genome of the laced fritillary *Argyreus hyperbius* (Lepidoptera: Nymphalidae). *Zoological Research*, **32**(5): 465-475.

Weller SJ, Pashley DP, Martin JA, Constable JL. 1996. Reassessment of butterfly family relationships using independent genes and morphology. *Annals of the Entomological Society of America*, **89**(2): 184-192.

Wolstenholme DR. 1992. Animal mitochondrial DNA: structure and evolution. *International Review of Cytology*, **141**: 173-216.

Xia X, Xie Z. 2001. DAMBE: Software package for data analysis in molecular biology and evolution. *Journal of Heredity*, **92**(4): 371-373.

Yang L, Wei ZJ, Hong GY, Jiang ST, Wen LP. 2009. The complete nucleotide sequence of the mitochondrial genome of *Phthonandria atrilineata* (Lepidoptera: Geometridae). *Molecular Biology Reports*, **36**(6): 1441-1449.

Yukuhiro K, Sezutsu H, Itoh M, Shimizu K, Banno Y. 2002. Significant levels of sequence divergence and gene rearrangements have occurred between the mitochondrial genomes of the wild mulberry silkworm, *Bombyx mandarina*, and its close relative, the domesticated silkworm, *Bombyx mori*. *Molecular Biology and Evolution*, **19**(8): 1385-1389.

Zou FZ, Hao JS, Huang DY, Zhang DX, Zhu GP, Zhu CD. 2009. Molecular phylogeny of 12 families of the Chinese butterflies based on mitochondrial ND1 and 16S rRNA gene sequences (Lepidoptera: Ditrysia: Rhopalocera). *Acta Entomologica Sinica*, **52**(2): 191-201. (in Chinese).

Differentiation in cranial variables among six species of *Hylopetes* (Sciurinae: Pteromyini)

Song LI^{1,2,*}, Fa-Hong YU³

1. Kunming Natural History Museum of Zoology, Kunming Institute of Zoology, Chinese Academy of Sciences, Kunming, Yunnan 650223, China

2. State Key Laboratory of Genetic Resources and Evolution, Kunming Institute of Zoology, Chinese Academy of Sciences, Kunming, Yunnan 650223, China

3. ICBR, University of Florida, Gainesville, FL 32610, USA

Abstract: There is some discrepancy in the classification of different species of *Hylopetes*, particularly regarding systematic status of *H. electilis* and *H. phayrei* and their relationship to other species. In the present study, for the first time we have brought together six of the nine *Hylopetes* species and performed statistical analysis of 14 measurable cranial variables, analyzing in total 89 specimens, including *H. electilis*, *H. alboniger*, *H. phayrei*, *H. lepidus*, *H. spadiceus*, and *H. nigripes*. Both univariate and multivariate analysis results indicate that *H. electilis* can not only be obviously distinguished from *H. phayrei*, but also clearly differs from the other four *Hylopetes* species. These results sustain the contention that *H. electilis* is neither a synonym nor subspecies of *H. phayrei*, but should be considered a distinct and valid species. Subsequently, a straightforward discussion on the biogeography of *Hylopetes* in southeastern Asia gives further insight into the differentiation and variety of species belonging to this genus.

Keywords: *Hylopetes*; Morphology; Cranial variables; Statistical analysis; Species

The genus *Hylopetes* (Thomas, 1908) mainly inhabits mountain forests in Asia, ranging from the Himalayas to the Greater Sunda Islands, and including areas of Nepal, China, Indochina, Philippines, Malaysia, and Indonesia (Corbet & Hill, 1992; Hoffmann et al., 1993; Nowak, 1999; Thorington & Hoffmann, 2005). Initially, *Hylopetes* was regarded as a subgenus of *Sciuropterus* (Thomas, 1908), but, based on Pocock's (1923) studies on the morphology of baculum, it was elevated to a full genus. This view, that the arrow-tailed flying squirrel *Hylopetes* in the eastern extreme of the Himalayas and southeastern Asia is a valid genus from the small Kashmir flying squirrel *Eoglaucomys* (A. H. Howell, 1915) in the western Himalayas, has been sustained by subsequent morphological and molecular studies (Nowak, 1999; Oshida et al., 2004; Thorington et al., 1996).

Based on several dental and cranial characteristics as well as external structures, different taxonomists have described varying numbers of *Hylopetes* species (Allen, 1940; Corbet & Hill, 1992; Ellerman, 1940; Ellerman & Morrison-Scott, 1950; Hoffmann et al., 1993; Nowak, 1999; Thorington & Hoffmann, 2005). To date, the maximal number of *Hylopetes* species was put at 13 (Ellerman, 1940), though the latest accepted result is 9

(Thorington & Hoffmann, 2005).

Allen (1940) described two subspecies of *Pteromys* (*Hylopetes*) *alboniger* (Allen, 1925), and listed the Hainan flying squirrel as *Pteromys electilis* (Allen, 1925). Ellerman (1940) listed 13 *Hylopetes* species, including *H. platyurus* (Jentink, 1890), *H. spadiceus* (Blyth, 1847), *H. phayrei* (Blyth, 1859), *H. alboniger* (Hodgson, 1836), and *H. nigripes* (Thomas, 1893) etc., but the Hainan flying squirrel from Namfong, Hainan Island, China was regarded as *Petromys electilis* (Allen, 1925). Ellerman & Morrison-Scott (1950) accepted the same results of *Petromys electilis* as Ellerman (1940), however, they listed only five *Hylopetes* species, including *H. spadiceus*, *H. phayrei*, *H. alboniger*, *H. fimbriatus* (Gray, 1837), and *H. sagitta* (Linnaeus, 1766). The last two species were emended in later studies: *H. fimbriatus* was listed as *Eoglaucomys fimbriatus* and *H. sagitta* was replaced by *H. lepidus* (Horsfield, 1822) in the results of Thorington &

Received: 22 December 2012; Accepted: 20 June 2013

Foundation items: This study was supported by the National Natural Science Foundation of China (30970332), Natural Science Foundation of Yunnan province (2007C099M).

* Corresponding author, E-mail: lis@mail.kiz.ac.cn

Hoffmann (2005). Corbet & Hill (1992) regarded *H. p. electilis* as subspecies of *H. phayrei*, and *Sciuropterus platyurus* was accepted as the synonym of *H. lepidus* (Horsfield, 1822), resulting in their listing of ten *Hylopetes* species, except for *H. fimbriatus* and *H. baberi* (Blyth, 1847), which were arranged as *Eoglaucomys fimbriatus*, and *H. platyurus* (Thorington & Hoffmann, 2005). The rest of the eight *Hylopetes* species were the same as the results of Thorington & Hoffmann (2005).

Despite lengthy and protracted debate, there remains several disagreements and uncertainties as to the taxonomy of this polymorphic genus. Among the most contentious include *H. electilis* in Hainan Island, China and *H. alboniger*, *H. phayrei*, *H. platyurus*, *H. spadiceus*, and *H. nigripes*, which have had a complicated taxonomic history due to intraspecific geographic variation in their distributions across Asia (Corbet & Hill, 1992; Hoffmann et al, 1993; Rasmussen & Thorington, 2008; Roberts, 1997; Thorington & Hoffmann, 2005). Despite the controversies, to date no attempt has been made to investigate the differences in measurable skull variables among these groups.

Morphometric data has been used to evaluate cranial, dental, and body measurements of various wild populations of mammals, and the resulting statistic analysis of variations on the morphological level has been proved useful in detecting patterns of geographic variations and delimiting intra- or inter-specific evolutionary units (Li et al, 2008; Li et al, 2012; Munoz & Perpinan, 2010; Slabova & Frynta, 2007; Zelditch et al, 2004). Because the specimens of *Hylopetes* are undoubtedly exiguous, we based our analysis on 89 specimens of 6 *Hylopetes* species. Principal components analysis (PCA) was performed to compare skull measurable variables among them, and furthermore, special attention was paid to the taxonomic status of Hainan flying squirrel from Namfong, Hainan Island, China, which has been listed as either a synonym or subspecies of *H. phayrei* (Corbet & Hill, 1992; Hoffmann et al, 1993; Thorington & Hoffmann, 2005).

MATERIALS AND METHODS

Samples

A total of 89 specimens of *Hylopetes* were examined and used for statistical analysis, including 39 females, 44 males, and 6 specimens of unknown sex (Appendix A). Adults were classified based on phalange ossification and dental patterns. All specimens used in this study were deposited in the American Museum of Natural History (New York, AMNH); the National Museum of Natural History (Washington DC, USNM); the Institute of Zoology, Chinese Academy of Sciences (IOZ, CAS) (Beijing, China); and the Kunming Natural History Museum of Zoology, Kunming Institute of Zoology (KNHMZ, KIZ, CAS) (Kunming, China). In total, 14 measurable cranial

variables (Figure 1) taken with a digital caliper to the nearest 0.01 mm were used in statistic analysis.

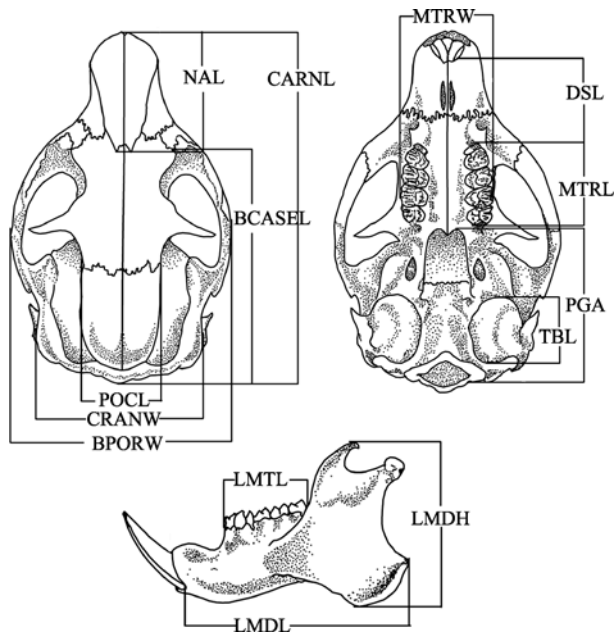


Figure 1 Measurements of 14 cranial variables used in the study

Data analysis

Statistical analysis of the morphometric study, which included sexual dimorphism, multiple comparisons, and principal component analysis (PCA) were performed using SPSS 11.0 (SPSS Inc., Chicago, USA). First, all variables were transformed into natural logarithms to eliminate the bias effect on large measurements in statistical analysis (D'elia & Pardinas, 2004). Then, Kaiser-Meyer-Olkin Measure of Sampling Adequacy (KMO) and Bartlett's Test were performed in order to test if the data were fit for analysis. Statistical differences were considered significant where $P<0.05$.

The Tests of Equality of Group Means (by Wilks' Lambda) was used to assess the sexual dimorphism of each group. In order to evaluate variations between samples, multiple comparisons (by Least-Significant Difference) between taxa were performed for all 14 cranial measurements. The associations between cranial measurable characters and species were assessed by multi-variate analysis of the PCA. PCA based on the variance-covariance matrix of the log-transformed variables was performed to identify variables that account for maximum variation in the data set, and to represent distances between major groups in order to assess the specific relationships among the individuals. The eigenvector scores describing the relative significance of each variable to principal components were used to compare the cranial morphological similarities and differences. The PCA scatter-plot visually represents the variation among different individuals of the samples (Figure 2).

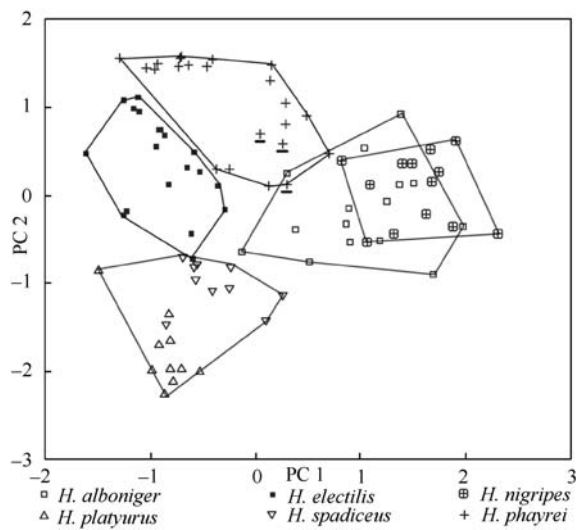


Figure 2 Plots of six *Hylopetes* species samples on the principal components factors 1 and 2

RESULTS

The means and standard deviation (*SD*) of 14 measurable cranial variables of *Hylopetes* are presented in Table 1. The results of KMO is 0.946 and that of *P* of Bartlett's Test of Sphericity is 0.000, together

confirming that the data gathered in the morphometric study were fit for PCA analysis. The Tests of Equality of Group Means for 83 samples showed no sexual dimorphism in all 14 cranial variables in the 6 *Hylopetes* species (Table 2). Table 3 presents the results of multiple comparisons on all 14 cranial variables between the species of *Hylopetes*.

Multivariate analysis was based on principal components analysis. In PCA, eigenvalues for the first three principal components were 12.161, 0.740 and 0.541 respectively, accounting for 96.014% of the total variance (Table 4). The first principal component factor (PC1) accounted for 86.867% of the total original variance and most variables had high positive loadings, suggesting the size variation in the samples. The second principal component (PC2) accounted for 5.284% of the total variance and is strongly correlated with TBL, with factor loadings >0.9. Along the third principal component factor (PC3), which accounts for 3.863% of the total variance, the main morphological variable contributing to this association is PORCL, with factor loadings >0.9.

Because the eigenvalue of the first principal components was 12.161, and the third was much lower (0.541), we used PC1 and PC2 to make the PCA scatterplot (Figure 2).

Table 1 Cranial variable measurements of *Hylopetes* (mean \pm SD)/range. Variable codes explained in Figure 1

Variables	<i>H. alboniger</i> <i>n</i> =15	<i>H. electilis</i> <i>n</i> =22	<i>H. nigripes</i> <i>n</i> =13	<i>H. platyurus</i> <i>n</i> =10	<i>H. spadiceus</i> <i>n</i> =10	<i>H. phayrei</i> <i>n</i> =19
CRANL	48.52 \pm 3.02 42.79–52.9	38.56 \pm 0.99 36.41–39.96	51.50 \pm 2.70 45.59–55.28	31.90 \pm 0.88 30.87–33.26	35.58 \pm 0.80 34.58–36.87	40.65 \pm 2.56 37.51–46.61
BCASEL	35.24 \pm 3.59 30.17–41.4	30.32 \pm 0.93 28.47–31.61	41.08 \pm 1.37 38.06–42.94	25.65 \pm 0.84 24.20–27.00	29.12 \pm 0.58 28.35–29.72	32.44 \pm 2.13 30.04–37.61
CRANW	21.98 \pm 0.62 20.97–22.98	18.21 \pm 0.44 17.44–18.93	22.58 \pm 0.52 21.93–23.46	16.38 \pm 0.39 15.81–17.02	17.67 \pm 0.29 17.33–18.35	18.84 \pm 1.12 17.13–20.91
BPORW	30.56 \pm 1.83 26.84–33.3	23.50 \pm 0.77 22.23–24.74	32.10 \pm 0.91 30.14–33.06	19.55 \pm 0.53 18.77–20.25	21.79 \pm 0.66 20.98–23.04	24.91 \pm 1.80 21.97–28.34
PORCL	11.51 \pm 0.79 10.07–12.89	11.20 \pm 0.65 9.84–12.41	11.71 \pm 0.77 10.06–13.10	9.78 \pm 0.52 9.23–10.63	10.20 \pm 0.57 9.38–11.26	10.10 \pm 0.64 9.03–11.50
PGA	19.63 \pm 1.37 17.11–21.34	15.42 \pm 0.60 14.35–16.17	20.79 \pm 0.96 18.40–22.00	13.66 \pm 0.44 13.12–14.58	15.40 \pm 0.64 14.20–16.64	16.65 \pm 1.20 15.43–19.07
NAL	14.35 \pm 1.36 11.90–16.20	10.66 \pm 0.72 9.27–12.22	16.17 \pm 0.85 14.14–17.42	9.06 \pm 0.41 8.18–9.53	10.15 \pm 0.48 9.37–10.93	11.67 \pm 1.13 9.97–13.94
TBL	8.79 \pm 0.52 8.20–10.16	8.55 \pm 0.51 7.52–9.25	9.30 \pm 0.46 8.63–9.96	6.64 \pm 0.30 6.31–7.21	7.40 \pm 0.17 7.12–7.59	9.43 \pm 0.47 8.45–10.14
DSL	10.21 \pm 1.06 8.12–11.64	8.15 \pm 0.40 7.42–8.95	10.46 \pm 0.77 8.53–11.81	6.42 \pm 0.38 5.97–6.98	7.33 \pm 0.40 6.39–7.80	8.79 \pm 0.77 7.53–10.48
MTRL	10.41 \pm 0.73 8.00–11.06	7.98 \pm 0.24 7.45–8.42	12.40 \pm 0.50 11.77–13.18	5.92 \pm 0.23 5.62–6.28	7.47 \pm 0.32 7.01–8.19	8.49 \pm 0.51 7.73–9.82
MTRW	12.86 \pm 0.54 11.89–13.97	9.96 \pm 0.28 9.35–10.45	12.96 \pm 0.29 12.46–13.44	7.74 \pm 0.27 7.32–8.03	8.66 \pm 0.40 8.27–9.55	10.33 \pm 0.56 9.42–11.60
LMDL	28.69 \pm 2.13 25.65–33.57	20.63 \pm 0.78 19.42–21.97	32.28 \pm 2.07 28.32–35.33	18.51 \pm 0.77 17.48–19.73	21.25 \pm 0.79 20.26–22.60	23.53 \pm 2.84 18.46–28.00
LMDH	18.42 \pm 1.56 14.41–20.22	14.22 \pm 0.62 13.36–15.42	21.05 \pm 1.20 19.06–22.80	11.38 \pm 0.64 10.38–12.34	13.02 \pm 0.64 12.01–14.01	14.82 \pm 1.09 13.61–17.55
LMTL	10.18 \pm 0.41 9.50–10.87	7.55 \pm 0.23 7.19–8.04	11.77 \pm 0.66 11.04–13.56	5.49 \pm 0.22 5.18–5.82	6.70 \pm 0.20 6.46–7.13	8.26 \pm 0.44 7.72–9.36

Figure 2 indicates PC1-PC2 scatter plots of principal component analysis. Inspection of Figure 2, samples of *H. electilis*, *H. platyurus*, *H. spadiceus*, and *H. phayrei* are distinguished from each other to form their distinct groups, showing different morphological characteristics of their skulls. However, results showed that samples of *H. alboniger* and *H. nigripes* are quite close to one another with considerable overlap, suggesting that *H. alboniger* shares similar measurable skull characteristics with *H. nigripes*. An interesting result was that the three samples named *H. electilis* from Chiang Mai, Thailand (labeled as “±” in Figure 2) are separated from those from Namfong, Hainan Island, but scatter in the samples of *H. phayrei*, hinting that the samples of *H. electilis* from Chiang Mai, Thailand should be more similar with those of *H. phayrei* in measurable skull characteristics.

DISCUSSION

Based on the specimens from Namfong, Hainan Island, China, Allen (1925) first described a valid species named *Pteromys (Petinomys) electilis*, but later on review classified it as *Pteromys electilis* (Allen, 1940). Later studies by Ellerman (1940) and Elleuman & Morrison-Scott (1950) continued to use *Petinomys electilis* as the scientific name for this species, and emphasized the species distribution on Hainan Island, China. However, based on their understanding of its two septa in each bulla, Corbet & Hill (1992) listed the group in *Hylopetes*. While Corbet & Hill (1992) narrated significant differences on pelage characteristics between

H. electilis and *H. phayrei*, they still opted to list it as belonging to *H. phayrei*, while placing *H. p. electilis* as its subspecies. More succinctly put, the validity of the Hainan flying squirrel, *H. electilis*, has been controversial for quite a long time (Corbet & Hill, 1991, 1992; Ellerman, 1940; Hoffmann et al, 1993; Nowak, 1999; Thorington & Hoffmann, 2005; Wang, 2003; Zhang et al., 1997).

The validity of various measurable cranial variables in distinguishing between species and species groups in *Hylopetes* has been critical in several studies. For example, Rasmussen & Thorington (2008) discussed the distributions for *H. platyurus*, *H. spadiceus*, and *H. Lepidus* using similar methods. In the present study, we performed statistical analyses on 14 measurable cranial variables from 22 samples of *H. electilis*, 19 of which came from Namfong, Hainan Island, China, in order to compare them with the samples of other five other validated *Hylopetes* species. The results showed significant difference between *H. electilis* and the other five *Hylopetes* species (Table 3), indicating it could be distinguished from other five species by using measurable skull variables. Similarly, though Figure 2 indicates that samples of *H. electilis* from Namfong, Hainan Island could be clearly distinguished from those of other five *Hylopetes* species, we found that they were closest to samples of *H. phayrei*, as opposed to the other four *Hylopetes* species. This result not only sustains the idea that *H. electilis* on Hainan Island should be a valid species, but it also may explain the reasons why there were so many systematic disagreements between *H. electilis* and *H. phayrei*.

Table 2 Tests of Equality of Group Means (by Wilks' Lambda) for Sexual Dimorphism

	Wilks' Lambda	F	df1	df2	P
CRANL	0.998	0.193	1	81	0.662
BCASEL	0.996	0.332	1	81	0.566
CRANW	1.000	0.022	1	81	0.884
BPORW	0.999	0.074	1	81	0.787
PORCL	0.995	0.443	1	81	0.507
PGA	0.999	0.090	1	81	0.765
NAL	1.000	0.038	1	81	0.846
TBL	1.000	0.000	1	81	0.991
DSL	0.996	0.308	1	81	0.580
MTRL	0.998	0.154	1	81	0.696
MTRW	1.000	0.008	1	81	0.930
LMDL	0.998	0.148	1	81	0.701
LMDH	0.992	0.645	1	81	0.424
LMTL	0.998	0.159	1	81	0.691

Variable codes are explained in Figure 1. Significant difference level: ** 0<P<0.001, * 0.001<P<0.05.

Table 3 Multiple Comparisons (by Least-Significant Difference) of all 14 cranial variables between the six *Hylopetes* species

	<i>H. alboniger</i> ~ <i>H. electilis</i>		<i>H. alboniger</i> ~ <i>H. nigripes</i>		<i>H. alboniger</i> ~ <i>H. platyurus</i>		<i>H. alboniger</i> ~ <i>H. spadiceus</i>		<i>H. alboniger</i> ~ <i>H. phayrei</i>	
	Mean difference	P	Mean difference	P	Mean difference	P	Mean difference	P	Mean difference	P
CRANL	0.097	0.000**	-0.029	0.001**	0.180	0.000**	0.131	0.000**	0.075	0.000**
BCASEL	0.063	0.000**	-0.068	0.000**	0.136	0.000**	0.081	0.000**	0.034	0.000**
CRANW	0.081	0.000**	-0.011	0.072	0.129	0.000**	0.094	0.000**	0.067	0.000**
BPORW	0.112	0.000**	-0.022	0.006*	0.193	0.000**	0.146	0.000**	0.088	0.000**
PORCL	0.014	0.120	-0.006	0.529	0.071	0.000**	0.054	0.000**	0.058	0.000**
PGA	0.103	0.000**	-0.024	0.008*	0.156	0.000**	0.106	0.000**	0.071	0.000**
NAL	0.126	0.000**	-0.053	0.000**	0.197	0.000**	0.149	0.000**	0.089	0.000**
TBL	0.010	0.165	-0.026	0.003*	0.120	0.000**	0.072	0.000**	-0.031	0.000**
DSL	0.096	0.000**	-0.010	0.418	0.200	0.000**	0.142	0.000**	0.065	0.000**
MTRL	0.113	0.000**	-0.077	0.000**	0.242	0.000**	0.142	0.000**	0.086	0.000**
MTRW	0.109	0.000**	-0.003	0.591	0.221	0.000**	0.172	0.000**	0.095	0.000**
LMDL	0.142	0.000**	-0.051	0.000**	0.187	0.000**	0.130	0.000**	0.087	0.000**
LMDH	0.111	0.000**	-0.059	0.000**	0.208	0.000**	0.150	0.000**	0.094	0.000**
LMTL	0.130	0.000**	-0.062	0.000**	0.270	0.000**	0.182	0.000**	0.092	0.000**
CRANL	-0.126	0.000**	0.083	0.000**	0.034	0.000**	0.021	0.001**	0.209	0.000**
BCASEL	-0.131	0.000**	0.073	0.000**	0.018	0.062	0.028	0.001**	0.205	0.000**
CRANW	-0.092	0.000**	0.047	0.000**	0.012	0.049*	0.014	0.005*	0.140	0.000**
BPORW	-0.135	0.000**	0.081	0.000**	0.034	0.000**	-0.023	0.001**	0.216	0.000**
PORCL	-0.021	0.033*	0.056	0.000**	0.039	0.000**	0.044	0.000**	0.077	0.000**
PGA	-0.128	0.000**	0.052	0.000**	0.002	0.800	-0.032	0.000**	0.180	0.000**
NAL	-0.179	0.000**	0.070	0.000**	0.022	0.082	-0.037	0.001**	0.250	0.000**
TBL	-0.037	0.000**	0.109	0.000**	0.061	0.000**	-0.042	0.000**	0.146	0.000**
DSL	-0.107	0.000**	0.103	0.000**	0.045	0.001**	-0.031	0.004*	0.210	0.000**
MTRL	-0.191	0.000**	0.128	0.000**	0.028	0.002*	0.027	0.000**	0.320	0.000**
MTRW	-0.113	0.000**	0.111	0.000**	0.062	0.000**	0.014	0.013*	0.225	0.000**
LMDL	-0.194	0.000**	0.045	0.001**	-0.011	0.362	0.055	0.000**	0.239	0.000**
LMDH	-0.171	0.000**	0.096	0.000**	0.038	0.001**	0.017	0.055	0.267	0.000**
LMTL	-0.192	0.000**	0.139	0.000**	0.051	0.000**	0.038	0.000**	0.332	0.000**
CRANL	0.160	0.000**	0.104	0.000**	-0.049	0.000**	-0.105	0.000**	-0.056	0.000**
BCASEL	0.150	0.000**	0.103	0.000**	-0.055	0.000**	-0.102	0.000**	-0.047	0.000**
CRANW	0.105	0.000**	0.078	0.000**	-0.035	0.000**	-0.062	0.000**	-0.027	0.000**
BPORW	0.169	0.000**	0.111	0.000**	-0.047	0.000**	-0.105	0.000**	-0.058	0.000**
PORCL	0.060	0.000**	0.065	0.000**	-0.017	0.162	-0.012	0.239	0.004	0.641
PGA	0.130	0.000**	0.096	0.000**	-0.050	0.000**	-0.084	0.000**	-0.034	0.000**
NAL	0.202	0.000**	0.142	0.000**	-0.048	0.002*	-0.108	0.000**	-0.060	0.000**
TBL	0.098	0.000**	-0.004	0.552	-0.048	0.000**	-0.151	0.000**	-0.103	0.000**
DSL	0.152	0.000**	0.075	0.000**	-0.058	0.000**	-0.134	0.000**	-0.076	0.000**
MTRL	0.220	0.000**	0.164	0.000**	-0.100	0.000**	-0.155	0.000**	-0.055	0.000**
MTRW	0.176	0.000**	0.099	0.000**	-0.049	0.000**	-0.126	0.000**	-0.077	0.000**
LMDL	0.182	0.000**	0.138	0.000**	-0.057	0.000**	-0.100	0.000**	-0.043	0.001**
LMDH	0.209	0.000**	0.154	0.000**	-0.058	0.000**	-0.113	0.000**	-0.055	0.000**
LMTL	0.244	0.000**	0.154	0.000**	-0.088	0.000**	-0.177	0.000**	-0.089	0.000**

Variable codes are explained in Figure 1. **: 0 < P < 0.001, *: 0.001 < P < 0.05.

Table 4 Factor loadings of the principal component analysis

Variables	PC1	PC2	PC3
CRANL	0.869	0.389	0.288
BCASEL	0.851	0.403	0.223
CRANW	0.875	0.262	0.346
BPORW	0.872	0.345	0.313
PORCL	0.295	0.112	0.945
PGA	0.910	0.307	0.214
NAL	0.912	0.284	0.214
TBL	0.373	0.915	0.107
DSL	0.775	0.523	0.214
MTRL	0.844	0.363	0.304
MTRW	0.801	0.416	0.367
LMDL	0.935	0.222	0.174
LMDH	0.886	0.326	0.279
LMTL	0.819	0.417	0.321
Eigenvalues	12.161	0.740	0.541
Variance explained (%)	86.867	5.284	3.863

Variable codes are explained in Figure 1.

Both a variety of previous studies as all as the present study have established that the Hainan flying squirrel, *H. electilis*, is restricted to Hainan Island, China (Ellerman, 1940; Ellerman & Morrison-Scott, 1950), and we thought that the channel isolation may have accelerated its absolute evolution. Based on molecular data, Jorgensen & Demarais (1999) and Oshida et al (2000) discussed the close genetic relationship and the recent divergence between *H. electilis* and *H. phayrei*. Their results suggest that these populations rapidly extended the ranges to their present distributions in a relatively short time (Jorgensen & Demarais, 1999; Oshida et al, 2000). Based on our current findings and the previous data, we recommend further correlative ecology studies on *H. electilis* and *H. phayrei* should be performed in order to gather more data that would help explain their adaptation process, and in doing so explain their phenotypic differentiation.

Additionally, three samples of *H. electilis* (labeled as “±” in Figure 2) from Chiang Mai, Thailand, were found to be not only clearly different from those of *H. electilis* from Namfong, Hainan Island, China, but they also scatter within samples of *H. phayrei* to form a close group (Figure 2). Based on the results of pelage comparison between *H. electilis* and *H. phayrei*, while Corbet & Hill (1992) listed the former as *H. p. electilis* while also emphasizing some significant differences in pelage characteristics between the two (Corbet & Hill, 1992). Our results also indicate that samples of *H. electilis* from Hainan Island could differ from those of *H. phayrei* samples from mainland in terms of skull

measurable characteristics (Figure 2), and likewise support their earlier results that *H. electilis* is distributed across Hainan Island, China. (Ellerman, 1940; Ellerman & Morrison-Scott, 1950).

The ultimate results from our statistical analysis of the skull characteristics sustains the argument that *H. electilis* is neither a synonym nor subspecies of *H. phayrei*, but a valid species in its own right. As for *H. platyurus*, although it was accepted as the synonyms of *H. lepidus* (Corbet & Hill, 1992), Figure 2 indicates that specimens of *H. platyurus* could be completely separated from five other *Hylopetes* species, similarly illustrating that it likely must also belong to a valid *Hylopetes* species. Unfortunately, without specimens of *H. lepidus* to serve as a comparison, the data collected in the present paper is suggestive but not conclusive, therefore we cannot definitively state whether *H. platyurus* is a synonym of *H. lepidus* or not. Further studies with more specimens may help further settle the ongoing debates regarding the taxonomy.

For a final note regarding geography, it is worth noting that *Hylopetes* are distributed in different zoogeographic subregions of the Oriental region, each with significant geographical variations (Corbet & Hill, 1992; Lekagul & Mcneely, 1988; Zhang et al, 1997). Accordingly, the samples of the six *Hylopetes* species used in this study can be morphologically distinguished as different, distinct groups (Figure 2). *H. alboniger* and *H. phayrei* belong to the Indochinese subregion and overlap extensively in Thailand, Indochina, Burma, and southern China (Corbet & Hill, 1992; Hoffmann et al, 1993; Thorington & Hoffmann, 2005), where the habitat is tropical, subtropical, or evergreen forest, with low elevation (500-1500 m) and within reach of southwest and south monsoons. Additionally, the population of *H. alboniger* occurs in the eastern extreme of the Himalayas and occupies temperate coniferous forest at mid elevations (1 500-3 000 m) or deciduous and subtropical forests at low elevations, while *H. nigripes* is endemic to the Philippines and occurs in subtropical or tropical dry forests (Nowak, 1999). Similar morphological characteristics (Figure 2) between *H. alboniger* and *H. nigripes* may potentially be adaptations to similar living habitats, though again, further studies are needed to explore this possibility.

South China itself is located at the crossroads of southeastern Asia, and has been a thoroughfare for animal dispersal from mainland Asia southward into the Indo-Malayan region. In southeastern Asia, many species have migrated south from Burma and southern China along the forested mountains of the Thai-Burma border into Malaysia, Sumatra, Java, and Borneo (Lekagul & Mcneely, 1988). *H. nigripes*, *H. lepidus*, and *H. spadiceus* inhabits the Sundaic sub region, with subtropical or tropical dry forests. The greatest distinction observed between *H. platyurus* and *H.*

spadiceus and other *Hylopetes* is consistent with discussions about *H. platyurus*, *H. spadiceus*, and *H. lepidus* by Rasmussen & Thorington (2008). However, because the habitats of these Sundaic *Hylopetes* are not well known and the ranges of these flying squirrels are poorly recorded, nearly every new collection will reveal new distribution limits, prompting further research. Based on that reality and the results of the present study, we suggest that future molecular studies on these species' phylogenies may give us more evidence as to the volition of their species status, and the subsequent estimation of divergence times will help us to understand the biogeography of *Hylopetes*, and perhaps give some further insight into larger shifts within the region.

Acknowledgments: We thank Andrew Willden of the Kunming Institute of Zoology for assistance with editing.

Appendix I

Specimens examined in this study

H. alboniger n=15

Yunnan, China: IOZ 5507 ♀, 5508 ♂, 15046 ♀; KIZ 00009 ♀, 76311 ♂, 84756, 89011, 90004, 206746, 206745, 640222 ♂, 640227 ♂; AMNH 114884 ♂, 114885 ♂, 114886 ♀;

H. electilis n=22

Hainan, China: AMNH 58138 ♀, 58158 ♀, 58159 ♀, 58160 ♂, 58161 ♀, 58162 ♂, 58163 ♂, 58164 ♀, 58166 ♀, 58167 ♂, 58171 ♂, 58172 ♂, 58176 ♂, 58179 ♀, 58180 ♂, 58181 ♂, 58182 ♀, 58186 ♀, 58198 ♂;

Chiang Mai, Thailand: AMNH 167891 ♀, 167892, 167893 ♂; *H. nigripes* n=13

Palawan, Philippines: AMNH 242098 ♀, 203314 ♀, 203313 ♂, 203311 ♀, 203309 ♂, 203310 ♂; USNM 477991 ♂, 477993 ♀, 477996 ♂, 478005 ♀, 478006 ♀, 478007 ♀, 478009 ♂;

H. platyurus n=10

Selamgger, W Malaysia: USNM 488617 ♀, 488619 ♀, 488620 ♂, 488623 ♂, 488624 ♀, 488625 ♀, 488626 ♀, 488630 ♂, 488631 ♂, 488633 ♂;

H. spadiceus n=10

Johore, W Malaysia: USNM 481109 ♂, 481110 ♀, 481112 ♀, 481114 ♂, 481116 ♂, 488648 ♂, 488638 ♂, 488641 ♀, 488645 ♀, 488646 ♀;

H. phayrei n=19

Banlad, Siam: USNM 294888 ♂, 294890 ♂, 294891 ♂, 294892 ♀, 297089 ♀;

Chiang Mai, Siam: USNM 260621 ♀, 260622 ♂, 260624 ♂, 153580 ♀;

Mandalaypopa, Burma: AMNH 163552 ♀, 163553 ♀, 163554 ♂, 163555 ♂, 163557 ♀, 163558 ♀, 163561 ♂, 163559 ♂, 163560 ♂, 163563 ♂.

References

Allen GM. 1940. The Mammals of China and Mongolia. Natural History of Central Asia. Vol. XI, Part 2. New York: American Museum of Natural History.

Corbet GB, Hill JE. 1991. A World List of Mammalian Species. 3rd ed. New York: Oxford University Press.

Corbet GB, Hill JE. 1992. The Mammals of the Indomalayan Region: A Systematic Review. New York: Oxford University Press.

D'ella G, Pardinas UFJ. 2004. Systematics of Argentinean, Paraguayan, and Uruguayan swamp rats of the genus *Scapteromys* (Rodentia, Cricetidae, Sigmodontinae). *Journal of Mammalogy*, **85**(5): 897-910.

Ellerman JR. 1940. The Families and Genera of Living Rodents with a List of Named Forms (1758 to 1936). Vol. I. London: British Museum (Natural History).

Ellerman JR, Morrison-Scott TCS. 1950. Checklist of Palaeartic and Indian mammals, 1758 to 1946. London: British Museum (Natural History).

Hoffmann RS, Anderson CG, Thorington RW Jr, Heaney LR. 1993. Family Sciuridae. In: Wilson D E, Reeder D M. Mammal Species of the World: Taxonomic and Geographic Reference. 2nd ed. Washington, D. C: Smithsonian Institution Press.

Jorgensen EE, Demarais S. 1999. Spatial scale dependence of rodent habitat use. *Journal of Mammalogy*, **80**(2): 421-429.

Lekagul B, Meneely JA. 1988. Mammals of Thailand. 2nd ed. Bangkok: Darnsutha Press.

Li S, Wang YX, Yang JX. 2008. Geographic variation of the Perny's Long-nosed squirrels (*Dremomys pernyi*) (Milne-Edwards, 1867) (Rodentia: Sciuridae) from southwestern China based on cranial morphometric variables. *Belgian Journal of Zoology*, **138**(1): 95-100.

Li S, Yu FH, Lü XF. 2012. Cranial morphometric study of four giant flying squirrels (*Petaurista*) (Rodentia: Sciuridae) from China. *Zoological Research*, **33**(2): 119-126.

Munoz FM, Perpinan D. 2010. Measurement error in morphometric studies: comparison between manual and computerized methods. *Annales Zoologici Fennici*, **47**(1): 46-56.

Nowak RM. 1999. Walker's Mammals of the World. 6th ed. Baltimore: Johns Hopkins University Press.

Oshida T, Lin LK, Yanagawa H, Endo H, Masud R. 2000. Phylogenetic relationships among six flying squirrel genera, inferred from mitochondrial cytochrome b gene sequences. *Zoological Science*, **17**(4): 485-489.

Oshida T, Shafique CM, Barkati S, Yasuda M, Hussein NA, Endo H, Yanagawa H, Masud R. 2004. Phylogenetic position of the small Kashmir flying squirrel, *Hylopetes fimbriatus* (= *Eoglaucomys fimbriatus*), in the subfamily Pteromyinae. *Canadian Journal of Zoology*, **82**(8): 1336-1342.

Pocock RI. 1923. The classification of Sciuridae. *Proceedings of the Zoological Society of London*, **1923**(1): 209-246.

Rasmussen NL, Thorington RW. 2008. Morphological differentiation among three species of flying squirrels (Genus *Hylopetes*) from Southeast Asia. *Journal of Mammalogy*, **89**(5): 1296-1305.

Roberts TJ. 1997. The mammals of Pakistan (revised edition). New York: Oxford University Press.

Slabova M, Frynta D. 2007. Morphometric variation in nearly unstudied populations of the most studied mammal: the non-commensal house mouse (*Mus musculus domesticus*) in the near East and Northern Africa. *Zoologischer Anzeiger: A Journal of Comparative Zoology*, **246**(2): 91-101.

Thorington RW Jr, Hoffmann RS. 2005. Family Sciuridae. In: Wilson E, Reeder DM. *Mammal Species of the World: Taxonomic and Geographic Reference*. 3rd ed. Washington, D.C.: The Johns Hopkins University Press.

Thorington RW Jr, Musante AL, Anderson CG, Darrow K. 1996. Validity of three genera of flying squirrels: *Eoglaucomys*, *Glaucomys*, and *Hylopetes*. *Journal of Mammalogy*, **77**(1): 69-83.

Thomas O. 1908. The nomenclature of the flying lemurs. *Annals and Magazine of Natural History*, **8**(1): 252-255.

Wang YX. 2003. A Complete Checklist of Mammal Species and Subspecies in China, A Taxonomic and Geographic Reference. Beijing: China Forestry Publishing House.

Zhang YZ, Jing SK, Quan GQ, Li SH, Ye ZY, Wang FG, Zhang ML. 1997. Muridae. In: Li W. *Distribution of Mammalian Species in China*. Beijing: China Forestry Publishing House.

Zelditch ML, Swiderski DL, Sheets HD, Fink WL. 2004. *Geometric Morphometrics for Biologists: A Primer*. New York: Elsevier Academic Press.

Three-dimensional morphology of the *Sinocyclocheilus hyalinus* (Cypriniformes: Cyprinidae) horn based on synchrotron X-ray microtomography

You HE^{1,*}, Xiao-Yong CHEN², Ti-Qao XIAO¹, Jun-Xing YANG^{2,*}

1. Shanghai Synchrotron Radiation Facility, Shanghai Institute of Applied Physics, Chinese Academy of Sciences, Shanghai 201204, China

2. State Key Laboratory of Genetic Resources and Evolution, Kunming Institute of Zoology, Chinese Academy of Sciences, Kunming 650223, China

Abstract: *Sinocyclocheilus* is a cave-dwelling cyprinid genus endemic to southwest China. Several species possess a conspicuous horn on their head, which has been suggested as a constructive troglomorphic trait but lacks substantial evidence. We used non-invasive, high spatial resolution synchrotron X-ray microtomography to investigate the three-dimensional (3D) morphology of the horn of *Sinocyclocheilus hyalinus*, one of eight such troglobiotic species. 3D renderings demonstrated the osteological components, which were comprised of a rear wall comprised of the supraoccipital bone, a remaining frontal wall with numerous fenestrae, and the bottom continuous with the parietal and epiotic. A horn cavity occurred within the horn. The fenestrae in the frontal wall were continuous in the horn cavity and showed elaborate channeling, and were, connected to the cranial cavity by soft tissue. We tentatively called this configuration the “otocornual connection” due to its anatomic and putative functional similarity to the otolateralic connection in clupeids and loricariids, which provide an indirect pathway to enhance perception of underwater sound signals. This study provides a functional morphology context for further histological and physiological investigations of such horn structures in *Sinocyclocheilus* cavefish, and we suggest that the horn might enhance acoustic perception to compensate for visual loss in subterranean life, which warrants future physiological examination as lab-reared *S. hyalinus* become available.

Keywords: *Sinocyclocheilus hyalinus*; Cavefish; Horn; Troglomorphism; Synchrotron X-ray microtomography

Abbreviations: C: cerebellum; Cc: cranial cavity; EPO: epiotic; F: frontal; Fo: foramen occipital; Foem: foramen occipital ellpticum magnum; FW: front wall of horn; Hc: horn cavity; LI: inferior lobe; MO: medulla oblongata; M: pd, muscle protractor dorsalis; OP: opercula; ot: optic tectum; P: parital; Pc: pharyngeal cavity; PG: pharyngeal bone; PT: pharyngeal teeth; PTE: pteroticSO: supraoccipital; TP: tripus; VC: valvula cerebella.

Cyprinid genus *Sinocyclocheilus* is endemic to China with more than 50 valid species (Zhao & Zhang, 2009). All species exhibit cave-dwelling behavior to different degrees. To survive in such extreme subterranean conditions, cavefish have evolved a suite of morphological and physiological characteristics (troglomorphic traits) in both regressive and constructive directions, such as loss of eyes and pigmentation and enhancement of mechanosensory and/or chemosensory perception (Jeffery, 2008, Poulsom, 2010; Wilkens, 2003). A sub-group of *Sinocyclocheilus* cavefish possess a conspicuous horn in

their head, which is unique among known cavefish worldwide. The horn has been suggested as a troglomorphic trait but without substantial evidence to support this (Romero et al, 2009). In addition, little is known in regards to its anatomy or function, partially due to the limited availability of such rare specimens. *Sinocyclocheilus hyalinus* Chen, Yang & Zhu (1994), “Tou ming jin xian ba (translucent golden-line barbel)”, is one such horn-containing, anophthalmic troglobiotic species (Chen et al, 1994). It was first reported from two specimens of 87 mm and 83.5 mm standard length, respectively. However, no further research has been

Received: 28 February 2013; Accepted: 12 April 2013

Foundation item: This work was partially supported by the fund of State Key Laboratory of Genetic Resources and Evolution (GREKF13-06)

* Corresponding authors, E-mail: yangjx@mail.kiz.ac.cn; heyou@sinap.ac.cn

reported in the past two decades. X-ray tomography has been applied in large and medium-sized fish osteological studies. The advent of synchrotron X-ray microtomography expands this application into fine structures and soft tissue morphology without any staining in millimeter-centimeter-sized specimens (Pasco-Viel et al, 2010; Boistel et al, 2011). Synchrotron X-rays have the advantage of high coherence suited to phase contrast imaging, an intense photon flux, and a monochromatic and parallel beam with micron/sub-micron spatial resolution.

In the present study, we employed synchrotron X-ray microtomography with 1.85-micron resolution to investigate the horn structure of one specimen of *S. hyalinus*. The resulting three-dimensional (3D) rendering and virtual section revealed the functional morphology of the horn. The resemblance of the horn configuration in the head of *S. hyalinus* and the “otolateralic connection” (such as recessus lateralis) in clupeids (Di Dario, 2004; Grande, 1985; Wilson et al, 2009) and loricariid catfish (Bleckmann et al, 1991; Schaefer & Aquino, 2000) suggest the possibility that the horn in *Sinocyclocheilus* fish might involve the enhancement of acoustic (and/or mechanosensory) perception.

MATERIALS AND METHODS

Specimen

One specimen of *S. hyalinus* measuring 41 mm standard length (Figure 1) was collected in February, 2009 from the Alu Ancient Cave (Luxi County, Yunnan Province), and was preserved in 10% formalin solution for about two years before the experiments. For the experiment, the specimen was switched to 70% ethanol solution and further dehydrated by gradient ethanol. A little shrinkage occurred after dehydration as indicated in the radiography (Figure 1). The horn was situated in the dorsal border between the head and trunk and displayed a forward protrusion.

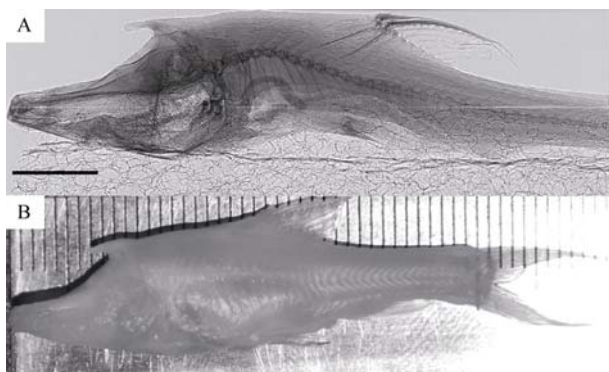


Figure 1 Radiography (A) and photography (B) of the examined specimen of *S. hyalinus*

Scale bar: 5 mm in A. One grid: 1 mm in B.

Synchrotron X-ray microtomography

The experiments were performed at the X-ray imaging beamline (BL13W1) at the Shanghai Synchrotron Radiation Facility (SSRF) in January and February, 2012. The *S. hyalinus* specimen was imaged by monochromatic synchrotron X-ray at 13.0 kV. The X-rays penetrating through the specimen were recorded as two-dimensional (2D) radiograph images (projection) by a charge coupled device (CCD) X-ray camera. The sample-to-detector distance was optimized for obtaining high in-line phase contrast. For synchrotron radiation X-ray microtomography (SR- μ CT) scanning, a PCO.2000 camera coupled with an optical magnification system (PCO AG, Kelheim, Germany) was used. In total, 720 projections, with 2s exposure time for each, were recorded during specimen rotation over 180°. Flat-field images and dark-field images were also collected during each acquisition procedure to correct electronic noise and variations in X-ray source brightness. The data were reconstructed into corresponding slices using the filtered back-projection algorithm (X-TRACT software, CSIRO). The 3D renderings were created from the stack of slices, and were manipulated and analyzed in VG Studio Max (v2.1) software.

During scanning, the specimen was held in a plastic tube vertically mounted on a sample stage. The synchrotron X-ray beam size was 45 mm (width) by 5 mm (height), so a 5 mm high segment including the horn was scanned using the 2X optical objective within the PCO.2000 camera. The local part containing the horn was then scanned using the 4X optical objective covering a height of 3.78 mm. The resulting spatial resolutions were 3.7 micron/pixel and 1.85 micron/pixel, respectively.

Additionally, a 2D radiography of the whole specimen (Figure 1) was stitched by two consecutive radiographies recorded using a VHR1:1 X-ray digital camera with direct coupled (micro) fiber-optic with 9 μ m/pixel resolution (Photonics Science Ltd, Robertsbridge, UK). The specimen was conventionally positioned in soft plastic foam on a sample stage, which vertically moved approximately 5 mm to allow the two consecutive radiographies.

RESULTS

Reconstructed 2D slice and 3D rendering

The original reconstructed slice from the SR- μ CT was an 8-bit grayscale image on the coronal plane. The mineralized tissue (pharyngeal teeth, vertebra, other bones), soft tissue (brain, musculature), and ambient air (cranial cavity, pharyngeal cavity) were easily distinguished from one another according to their different gray values (Figure 2A, C). The mineralized tissues with high grey values were white in the reconstructed slices, whereas air with the lowest value was dark. The 3D rendering was

created in VG Studio software using the stack of slices, from which sagittal and horizontal virtual sections could be further created (Figure 2C). By increasing grey pixel value, the pixel below or equal to the set threshold was interpreted as black. Such manipulation allowed for the

virtual removal of the soft tissue (“virtual corrosion”), and demonstrated the osteological components (Figure 2B, D–I). Areas with the same grey value could be delimitated and labeled in designated colors, thus the potential cavity inside the specimen could be labeled.

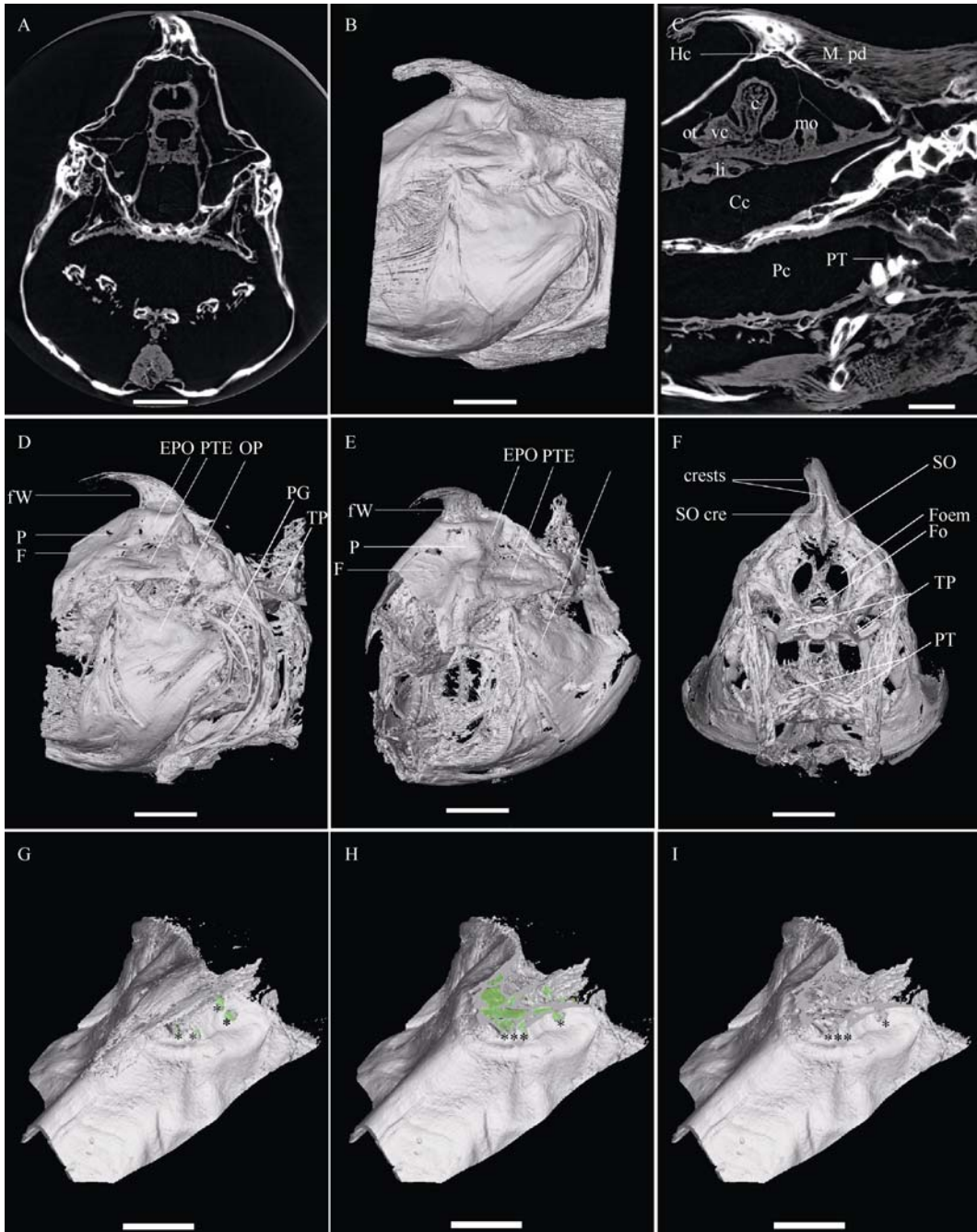


Figure 2 2D reconstructed slices and overall 3D rendering of the horn

Each reconstructed coronal and sagittal slice is presented (A, C), where bones, soft tissue, and air-filled cavities are distinguished from each other by different grey values. Overall 3D rendering (B) was created from the stack of original reconstructed coronal slices. After virtual removal of musculature and other soft tissue, the osteological components are displayed in lateral, oblique, and rear view (D–F). A–F are from SR- μ CT scanning at 3.7-micron resolution. G–I are from scanning at 1.85-micron resolution. The top part of the horn remains in G, but is removed in H and I to display the bony bottom of the horn. The horn cavity is labeled in pale green. H and I differ in whether the remaining horn cavity is labeled or not. A star marks the fenestrae on the frontal wall. Scale bar: 1 mm in A; 1.5 mm in B, D–F; 0.85 mm in C, G–I.

General 3D morphology of the horn

To observe the overall 3D morphology of the horn, a 3D rendering of a 5-mm segment containing the otic region and the horn was created (Figure 2B). The horn was situated at the dorsal otic region of the skull and bent forward as a protrusion with a flattened ending. After virtual removal of musculatures and other soft tissues, the osteological components of the horn were presented, which were divided into rear wall, remaining frontal wall, and bottom. The supraoccipital (SO) bone provided the rear wall (Figure 2F), at which the hypertrophy muscle protractor dorsalis (M.pd) was attached (Figure 2C). The supraoccipital crest and two additional crests on both

sides formed along the suture between the SO and dorsal-posterior parts of the remaining frontal wall (fW) (Figure 2F). The fW, bearing numerous fenestrae, arose from the parietal and epiotic (Figure 2D, E). The bottom was continuous with the parietal and the epiotic, but we were unable to identify whether the parietal or the epiotic formed the bottom. The SO and the fW merged at the distal ending and separated at the basal part of the horn. Thus, a cavity was formed within the horn, and the channeling of the fenestrae in fW connected to it was more elaborate. The horn cavity was labeled in pale green in individual panels (Figures 2 and 3), and further demonstrated the following.

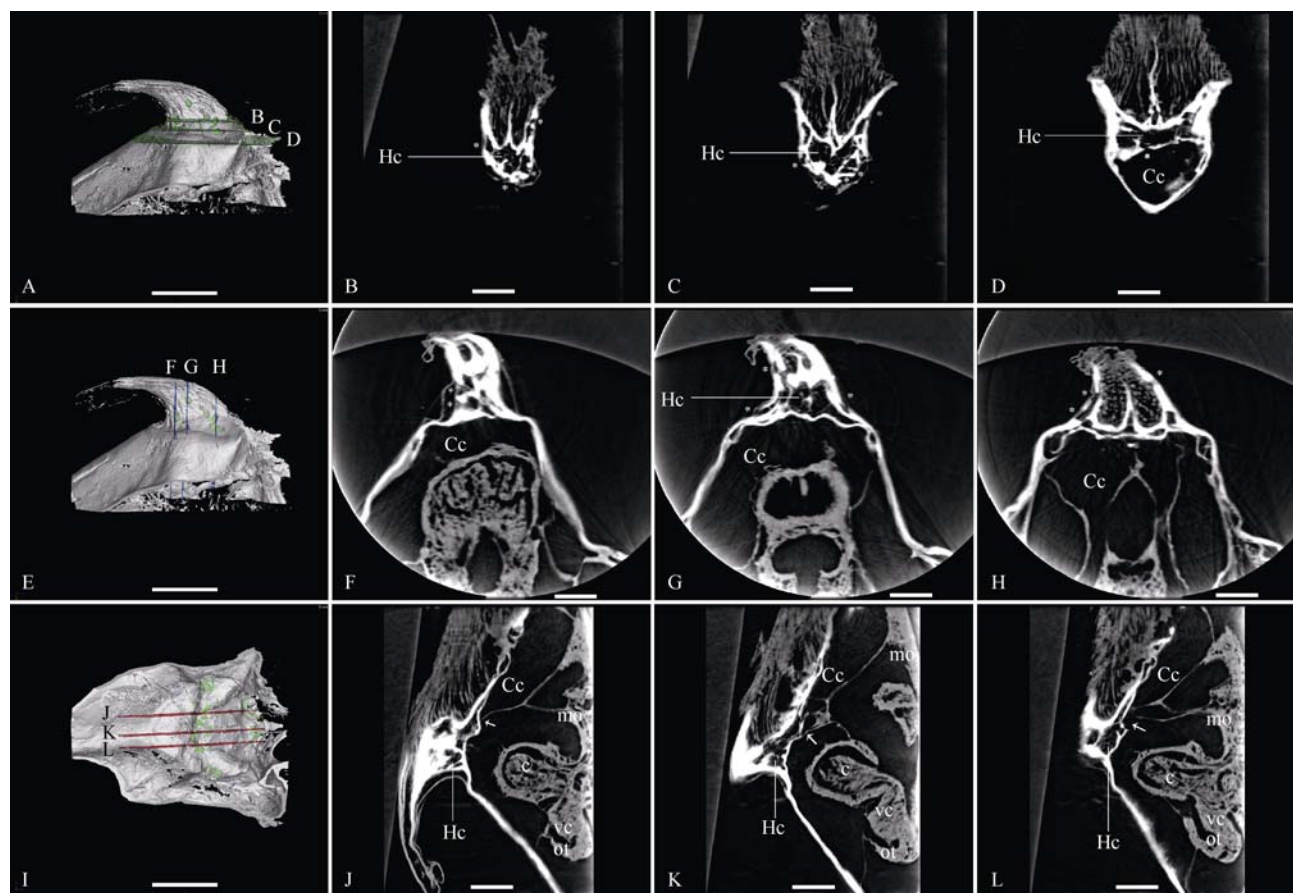


Figure 3 Connecting pathway “frontal wall bearing elaborate fenestrae→horn cavity with soft tissue connection→cranium” revealed in representative horizontal (B–D), coronal (F–H), sagittal (J–L) sections

In the two upper horizontal sections, the horn cavity with trabeculae-like structure and the fenestrae with elaborating channeling are most evident (B, C), while in the lowest horizontal representative section the cranium appears and the bony bottom with one foramen is also shown (D). In the coronal sections, the cranial cavity containing part of cerebellum is evident, and elaborate channeling of fenestrae is also visible (F, G); the horn cavity almost disappears in the posterior representative section (H). The fenestrae and foramen are indicated with a star. In sagittal sections, the soft tissue, which arose from the dorsal medulla oblongata and connected the horn and cranial cavities, are most evident, and the foramen position through which the connection penetrated are indicated by arrows (J–K). Skin tissue investing the horn is also displayed (Figure 3B–D, F, G, J). In each row, the position of the representative sections are indicated in the left most panels, where the horn cavity labelled in pale green is visible through the fenestrae in fW or the foramen in the bony bottom (A, E, I). All images are from SR-μCT at 1.85-micron resolution. Scale bar: 1.1 mm in A, E, I; 0.55 mm in B–D, J–L; 0.4 mm in F–H.

Configuration of “otocornual connection”

To better demonstrate details, a 3D rendering from an additional SR- μ CT scan at 1.85-micron resolution was created. In the oblique view, the horn cavity from the cranial cavity was evident after removal of the top part of the horn (Figure 2G–I), especially through comparison between the images with and without labeling of the remaining horn cavity (Figure 2H–I). Several foramen in the bony bottom were evident from the ventral view, through which the horn was connected to the cranial cavity (Figure 3I).

Furthermore, sagittal, coronal, and horizontal virtual sections were performed. A configuration, tentatively called the “otocornual connection”, was resolved from these sections. In general, the fenestrae in fW showed elaborate channeling and were continuous with the horn cavity, which in turn was connected with the cranial cavity by soft tissue. The horn cavity and fenestrae with elaborate channeling were most evident in the representative horizontal sections (Figure 3B–D), but were also easily identified in the sagittal and coronal sections where the fenestrae were labeled with a star (Figure 3F, 3G, 3J–L). The soft tissues forming the connection between the horn and cranial cavity were

evident in the representative sagittal sections, which arose from the dorsal medulla oblongata and penetrated into the horn cavity through the bony bottom (indicated by arrows in Figure 3J–L). Unfortunately, we were unable to further identify whether the soft tissue connecting the two cavities was neural or membrane tissue based on the grey value in the image. The trabeculae-like soft tissues (or connective tissue) were also visible in the horn cavity in the horizontal and sagittal sections (Figure 3B, C, K, L). The cerebellum, otic tectum and part of the medulla of the brain with certain decay were also shown in the sagittal sections (Figure 3J–L).

To give an intuitive presentation, two modified 3D renderings were created with the horn cavity labeled in pale green, and the cerebellum and otic tectum labeled in khaki-grey as a reference for the cranium (Figure 4). In one 3D rendering, the encasing structures were set in semitransparent status to emphasize the horn cavity and brain tissue (Figure 4A). In the other rendering, the left half encasing structure was removed to exposure the horn and cranial cavity, where the connecting soft tissue was visible and appeared to be membrane rather than fiber tissue (Figure 4B).

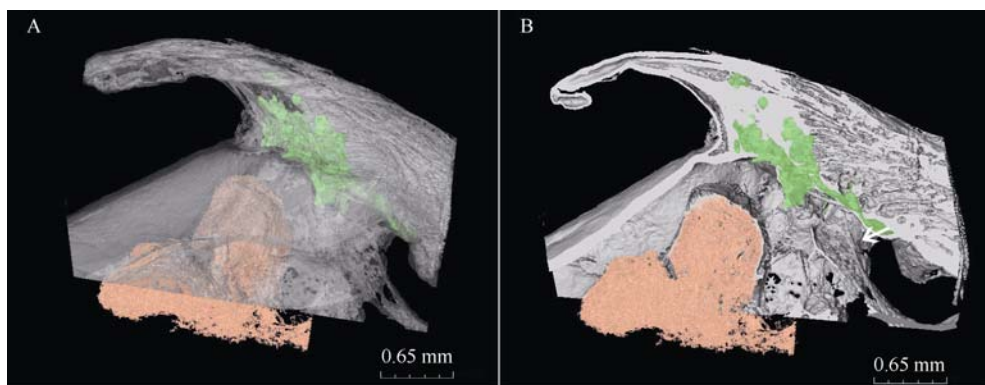


Figure 4 Two 3D renderings for the intuitive presentation of the “otocornual connection” configuration. The horn cavity is labeled pale green, and the cerebellum and otic tectum khaki-grey. The encasing structure is semitransparent in A, whereas the left half encasing structure is removed to exposure the horn cavity and cranium in B. The connecting soft tissue is indicated by an arrow in B.

The “otocornual connection” might provide a “frontal wall bearing elaborate fenestrae → horn cavity with soft tissue connection → cranium” pathway, with its potential function discussed in next section.

DISCUSSION

We employed a non-invasive SR- μ CT approach to investigate a *S. hyalinus* specimen at resolution of 1.85-microns, and revealed the osteological components and “otocornual connection” configuration of the horn. The 3D morphology results will help clarify previous reports in relation to anatomic structure, and provide evidence

about the possible function of the horn to enhance acoustic perception to compensate for visual loss in cave life.

The *Sinocyclocheilus* horn is unique among all known troglobiotic species. Eight troglobiotic species, namely *S. angularis*, *S. aquihornes*, *S. bicornutus*, *S. broadihornes*, *S. furcodorsalis*, *S. hyalinus*, *S. rhinoceros*, and *S. tileihornes*, possess these horny protrusions. Wang et al (1999) delineated the horn of *S. angularis* and *S. bicornutus* as a whole parietal protrusion without supraoccipital or other osteological components, which was concluded in subsequent literature that the horn consisted of the frontal and

parietal bones. Li et al. (2002) performed gross anatomy on *S. rhinoceros* and concluded that the horn was composed of three ossicles set perpendicular to one another. Our 3D morphology results showed that the supraoccipital bone and ossicles arose from the parietal and epiotic, and a bony bottom comprised the osteological base of the horn. These results indicated that the frontal did not build the horn structure, and disagreed with previous findings that the horn is a “whole parietal protrusion”. The explanation that the three ossicles are set perpendicular to one other in *S. rhinoceros* seems to be an incorrect interpretation of the three crests (supraoccipital crest and two additional crests on both sides formed by suture of the supraoccipital and posterior edge of the front wall) found in the rear wall in *S. hyalinus*. Recently, molecular phylogenetic analysis has indicated that all examined horn-possessing species are clustered within one monophyletic clade (Xiao et al., 2005; Li et al., 2008), called the “angularis” clade (Zhao et al., 2009). Systematic investigation of the 3D morphology of horns and analysis of the conservation and variation among them would benefit our understanding of evolution within this “angularis” clade.

The horn has been suggested as a possible troglomorphic characteristic for *Sinocyclocheilus* cavefish (Romero et al., 2009), but whether this structure is related to adapted subterranean life, the function of the horn, and how it contributes to sensory perception are still unknown. From the 3D morphology, it is tempting to speculate that the horn might be an adaptation to enhance acoustic perception. Underwater sound has two physical components, particle motion and sound pressure wave. All fish can detect particle motion through inertial movement between the otolith and sensory epithelia within the inner ear. Some fish can also detect sound pressure by physical connection structures transforming sound pressure into the inner ear (Popper, 1993, 2011). In otophysans, the Weberian ossicles connect the swim bladder and otic capsule. The swim bladder inside the abdominal cavity is set into motion by pressure in the sound field, and such vibrations are transformed by Weberian ossicles into particle motion perceived by the inner ear. In clupeids, the complex *recessus lateralis* structure in the otic region of the skull is an intracranial space into which the supraorbital, infraorbital, preopercular and temporal sensory canals open (Grande, 1985; Di Dario, 2004). A pair of gas-filled auditory bullae in clupeid heads directly contacts the *recessus*

lateralis at the lateral side and the modified utricle at the medial side. Proper configuration of the *recessus lateralis*, auditory bullae and modified utricle provides an indirect pathway for the pressure component of sound to be perceived by the inner ear of certain clupeid species. *Recessus lateralis* lesions or filling auditory bullae with ringer solution has been shown to damage the ability to detect 40 kHz sounds in Gulf menhaden (Wilson et al., 2009). In loricariid, a similar structure is also found in the temporal region of the skull, where a section of the posotic laterosensory canal deep within the ventral layer of the compound pterotic is in direct contact with the horizontal canal of the inner ear (Bleckmann et al., 1991; Schaefer, 2000). These “pressure transducer” otophysical connections in otophysans and otolateralic connections in clupeids improve hearing capability (such as auditory sensitivity, frequency bandwidth, and sound source location). In the present 3D rendering of *S. hyalinus* horn, a “frontal wall bearing elaborate fenestrae→horn cavity with soft tissue connection→cranium” configuration was clearly revealed, which was tentatively named the “otocornual connection” due to its anatomical and putative functional similarity to otophysical and otolateralic connections, which enhance sound pressure perception. Acoustic perception could be particularly important in the subterranean lightless environment of blind cavefish. Whether the horn functions to enhance acoustic perception warrants future physiological studies as lab-reared *S. hyalinus* become available.

In conclusion, we demonstrated the presence of a cavity inside the horn of *S. hyalinus* with a connection to the cranium. The supraoccipital bone provides the rear wall of the horn, and the remaining frontal wall bears numerous fenestrae. Such a configuration implies a potential putative function as an indirect pathway to perceive sound pressure. This study also provides a functional morphological context for further anatomic and functional investigations of horn structures found in Chinese *Sinocyclocheilus* cavefish.

Acknowledgements: You HE is grateful to Prof. Meeman CHANG (Institute of Vertebrate Paleontology and Paleoanthropology) and Prof. Jiakun SONG (Shanghai Ocean University) for motivating his interest in fish functional morphology. Authors also thank them and Dr. Ning WANG (Institute of Vertebrate Paleontology and Paleoanthropology) for their helpful discussion.

References

Bleckmann H, Niemann U, Fritzsch B. 1991. Peripheral and central aspects of the acoustic and lateral line system of a bottom dwelling catfish, *Ancistrus* sp. *The Journal of Comparative Neurology*, **314**(3): 452–466.

Boistel R, Swoger J, Krzic U, Fernandez V, Gillet B, Reynaud EG. 2011. The future of three-dimensional microscopic imaging in marine biology. *Marine Ecology*, **32**(4): 438–452.

Chen YY, Yang JX, Zhu ZG. 1994. A New fish of the genus *Sinocyclocheilus* from Yunnan with comments on its characteristic adaption (Cypriniformes: Cyprinidae). *Acta Zootaxonomica Sinica*, **19**(2): 246-253. (in Chinese)

Di Dario F. 2004. Homology between the *recessus lateralis* and cephalic sensory canals, with the proposition of additional synapomorphies for the Clupeiformes and the Clupoidei. *Zoological Journal of Linnean Society-Lond*, **141**(2): 257-270.

Grande L. 1985. Recent and fossil Clupeomorph fish with materials for revision of the subgroups of Clupeoids. *Bulletin of the American Museum of Natural History*, **181**(2): 235-372.

Jeffery WR. 2008. Emerging model systems in evo-devo: cavefish and microevolution of development. *Evolution and Development*, **10**(3): 265-272.

Li W, Tao J. 2002. Local dissection of body of the fishes *Sinocyclocheilus rhinoceros*. *Journal of Yunnan Agricultural University*, **17**(3): 207-209. (in Chinese)

Li ZQ, Guo BC, Li JB, He SP, Chen YY. 2008. Bayesian mixed models and divergence time estimation of Chinese cavefishes (Cyprinidae: *Sinocyclocheilus*). *Chinese Science Bulletin*, **53**(15): 2342-2352.

Pasco-Viel E, Charles C, Chevret P, Semon M, Tafforeau P, Viriot L, Laudet V. 2010. Evolutionary trends of the pharyngeal dentition in cypriniformes (*Actinopterygii: Ostariophysi*). *PLoS One*, **5**(6): e11293.

Popper AN, Fay RR. 1993. Sound detection and processing by fish—critical review and major research questions. *Brain Behavior and Evolution*, **41**(1): 14-38.

Popper AN, Fay RR. 2011. Rethinking sound detection by fishes. *Hearing Research*, **273**(1-2): 25-36.

Poulson TL. 2010. Cavefish: Retrospective and Prospective. In: Trajano E, Bichuette ME, Kapoor BG. *Biology of Subterranea Fishes*. Enfield: Science Publishers, 1-39.

Romero A, Zhao YH, Chen XY. 2009. The Hypogean fishes of China. *Environmental Biology of Fishes*, **86**(1): 211-278.

Schaefer SA, Aquino AE. 2000. Postotic laterosensory canal and pterotic branch homology in catfishes. *Journal of Morphology*, **246**(3): 212-227.

Wang DD, Chen YY, Li XY. 1999. An analysis on the phylogeny of the genus *Sinocyclocheilus* (Cypriniformes: Cyprinidae). *Acta Academiae Medicinae Zunyi*, **22**(1): 1-6. (in Chinese)

Wilkens H, Strecker U. 2003. Convergent evolution of the cavefish *Astyanax* (Characidae, Teleostei): genetic evidence from reduced eye-size and pigmentation. *Biological Journal of the Linnean Society*, **2003**, **80**(4): 545-554.

Wilson M, Montie EW, Mann KA, Mann DA. 2009. Ultrasound detection in the Gulf menhaden requires gas-filled bullae and an intact lateral line. *Journal of Experimental Biology*, **212**(21): 3422-3427.

Xiao H, Chen SY, Liu ZM, Zhang RD, Li WX, Zan RG, Zhang YP. 2005. Molecular phylogeny of *Sinocyclocheilus* (Cypriniformes: Cyprinidae) inferred from mitochondrial DNA sequences. *Molecular Phylogenetics and Evolution*, **36**(1): 67-77.

Zhao YH, Zhang CG. 2009. Endemic Fishes of *Sinocyclocheilus* (Cypriniformes: Cyprinidae) in China. Beijing: Science Press.

Effects of Zn²⁺ and Cu²⁺ on loach ovaries and ova development

Jian-Xun TANG^{1,*}, Jun-Rong LI¹, Zhong-Liang LIU¹, Hua ZHAO¹, Xiao-Min TAO², Zhang-Shun CHENG²

1. College of Agriculture and Bio-engineering, Jinhua Polytechnic Institute, Jinhua, 321007, China

2. College of Pharmacy and Material Engineering, Jinhua Polytechnic Institute, Jinhua, 321007, China

Abstract: This study compared the accumulation of Zn²⁺ and Cu²⁺ in the ovaries and ova of loaches under different concentrations of Zn²⁺ (1.00, 2.50 and 5.00 mg/L respectively) and Cu²⁺ (0.10, 0.25 and 0.50 mg/L respectively). The results showed that both Zn²⁺ and Cu²⁺ accumulated in the ovaries, and that the relationship between accumulation and time was linear over 20 days of exposure. The accumulation of the metals in ovaries was closely related to the concentration of exposure in the solutions ($P<0.05$), and was obviously affected by the time and doses. However, the Cu²⁺ concentration was significantly higher than Zn²⁺ ($P<0.05$). The development level of ova in the ovaries also correlated with the concentration and exposure period in the Zn²⁺ and Cu²⁺ solutions.

Keywords: *Misgurnus anguillicaudatus*; Ovary; Ovum; Zn; Cu; Accumulation

The problem of heavy metal pollution in aquatic environments has become an increasingly serious concern over the past decades in China (Wang et al, 2008). The resulting pollution that accompanies industrialization has severely challenged the survival of aquatic animals due to strong toxicity and the bioaccumulation of heavy metals. Of these pollutants, metal ions accumulate not only in the skin, muscles, liver, and kidneys (Al-Weher S et al, 2008; Dutta T et al, 2001; Has S et al, 2008; Migliarini et al, 2005), but also in the gonads, which poses a serious threat to the reproductive success of many aquatic species and by extension the overall population of those animals (Abou El-Naga et al, 2005; da Cruz et al, 2007; Tang et al, 2010). Accordingly, to maintain biodiversity and protect the breeding system of aquatic fauna, it is necessary to conduct studies on the accumulation of heavy metals in a fish's reproductive organs and the resulting stress on their ova to thereby establish correlations between metal accumulation and ion concentration.

Zn²⁺ and Cu²⁺ are commonly found in bodies of water polluted by heavy metals. Neither biodegrades easily and these metals are amplified via bioaccumulation as they pass through food chain. To explore how heavy metal accumulation strains the development of the ovaries and ova, in this study we used Loaches (*Misgurnus*

anguilllicaudatus), a fish species known to tolerate pollution well (Gao et al, 2003; Wang et al, 2003) as a model. By doing so, we hope to find results that will prove useful in gauging the impact assessment of aquatic organisms, diagnostics of environmental pollution, and biodiversity conservation.

MATERIALS AND METHODS

Animal specimens and reagent materials

Two year old loaches ($n=220$) were purchased from a local farmer's market for use as a testing species. The overall mean length of the fish was 13.2 ± 3.5 cm and the mean body weight 37 ± 0.48 g.

Concentrated solutions (1 000 mg/L) of ZnSO₄ (AR) and CuCl₂ (GR) were first prepared before being diluted into the corresponding concentrations as needed throughout the course of the experiment. HNO₃ (AR) and HCIO₄ (AR) were mixed at a ratio of 4:1 before use.

Instruments and equipments

The following equipment were used over the duration

Received: 28 February 2013; Accepted: 06 June 2013

Foundation item: Natural Science Foundation of Zhejiang (LY12C03006), China

* Corresponding author, E-mail: jhtjxun@163.com

of this study: an H-6800 Aerating Pump (China); an IRIS Intrepid ER/S-model ICP atomic emission spectrometer (Thermo Elemental Co., USA); a CKX41 inverted fluorescent microscope (HQ2592×1944) (Olympus Co., Japan); an LSP far-infrared cooking stove (China); a KD (freeze) slicing machine (China); and a DGG-9070A drying oven with an electrical thermostatic wind drum (China).

Experimental design

The experiment was carried out indoors. During testing, the water quality parameters were maintained consistently: pH 6.3–6.5, DO 5.1–6.2 mg/L; temperature at 8–12°C (measured daily); average total water hardness at 2.67 mmol/L; and average alkalinity at 2.6 mmol/L.

Polyethylene plastic aquariums (40 cm×30 cm×45 cm) were used as exposure devices, and 20 L of tap water, in which no Zn²⁺ and Cu²⁺ was detected, was added to each tank and then aerated for more than 2 days prior to being used. The loaches accepted for testing were visually inspected to be disease-free, injury-free and active, with an overall mortality rate less than 5% during the testing period. The fish were acclimated to lab conditions for 5 days before the experiment began. Over the course of testing, there was no water exchange in the plastic aquariums and the fish were not fed. An aerating pump was used to keep dissolved oxygen above 5 mg/L.

In total, 220 similarly sized loaches were randomly placed into four testing groups. The control group was placed in water with no heavy metals present, while the other three were given different concentrations of Zn²⁺ and Cu²⁺ similar to actual ion concentrations in the local water bodies based on the Chinese Standard of Water Quality for Fisheries (GB11607-1989): Zn²⁺ concentrations of 1.00, 2.50 and 5.00 mg/L paired with Cu²⁺ concentrations of 0.10, 0.25 and 0.50 mg/L. The fish were held in each aquarium and three parallels for each concentration over the course of the 20-day experiment. Each individual was weighed, boiled, and dried prior to analysis, during which ovary slices from

different groups and at different times (before testing, 5-day, 10-day and 20-day) were cut and observed.

Statistical analysis

The processing method of statistics for the testing results follows the method described by Nan Xu-Yang (Nan, 2009). All data was analyzed using SPSS 11.0 data processing system (SPSS Inc., Chicago, USA) for analysis of variance. The values for individual experiments were collected to calculate the mean value and the standard deviation/error to make comparisons. The statistical significance of the difference between means was determined using one-way ANOVA, with $P<0.05$ being statistically significant.

RESULTS

Accumulating rule of Zn²⁺ and Cu²⁺ in ovaries

Before exposure to the metals, Zn²⁺ and Cu²⁺, all loaches were tested to ensure that no metals were present in the ovaries. By 10 days of exposure, the concentrations of Zn²⁺ and Cu²⁺ in loach ovaries across all groups being kept in water with varying concentrations of heavy metals had increased. On day 20, the concentration of both ions showed an increasing trend, but between day 10 and day 20 the concentrations of Zn²⁺ and Cu²⁺ in the ovaries seemed to decline significantly when compared to ion concentrations of the groups when they had been exposed for less than 10 days ($P<0.05$).

The cumulative capacity of Zn²⁺ and Cu²⁺ in the ova was positively related to concentration of the metals in aqueous solution ($P<0.05$). The accumulation of Zn²⁺ and Cu²⁺ in the ovaries presented as a function of exposure time and dose effects are shown in Table 1. In the control group, no Zn²⁺ and Cu²⁺ were detected.

Table 2 shows the regression equations and correlation coefficients for ovaries, indicating a positive relationship between Zn²⁺ and Cu²⁺ accumulation and exposure time. Relationships between accumulation of Zn²⁺ and Cu²⁺ in the ovaries and exposure time are shown in Figures 1 and 2.

Table 1 Accumulation of Zn²⁺ and Cu²⁺ in ovary at different time intervals ($n=200$)

Time (d)	Treatment	Zn ²⁺ / Cu ²⁺ in solution (mg/L)	Zn ²⁺ (μg/g; dry wt)	Cu ²⁺ (μg/g; dry wt)
5	control	—	—	—
	group 1	1.00 / 0.10	1.3±0.4 ^e	3.4±0.2 ^e
	group 2	2.50 / 0.25	2.5±0.4 ^{fg}	5.6±0.8 ^g
	group 3	5.00 / 0.50	3.6±0.7 ^{def}	8.9±0.9 ^g
10	control	—	—	—
	group 1	1.00 / 0.10	2.3±0.7 ^{ef}	54.3±2.5 ^f
	group 2	2.50 / 0.25	5.1±0.2 ^d	81.5±4.7 ^e
	group 3	5.00 / 0.50	26.4±1.7 ^b	145.33±5.6 ^b
20	control	—	—	—
	group 1	1.00 / 0.10	4.3±0.3 ^{de}	117.1±6.7 ^d
	group 2	2.50 / 0.25	7.6±0.4 ^c	137.2±11.0 ^c
	group 3	5.00 / 0.50	39.1±3.2 ^a	329.3±18.4 ^a

Different superscripts show significant difference ($P<0.05$), while the same superscript shows no significance ($P>0.05$) between groups.

Table 2 Regression equations and coefficients of accumulation for Zn²⁺ and Cu²⁺ with exposure time in ovary

Treatment	Heavy metal	Regression equation	Correlation coefficient (R^2)
group 1	Zn	$y=0.185x+0.7408$	0.7834
	Cu	$Y=9.3235x-30.158$	0.9543
group 2	Zn	$y=0.3254x+1.2608$	0.9355
	Cu	$Y=9.3654x-15.307$	0.8286
group 3	Zn	$y=2.2072x-2.7333$	0.8648
	Cu	$y=24.754x-87.721$	0.9716

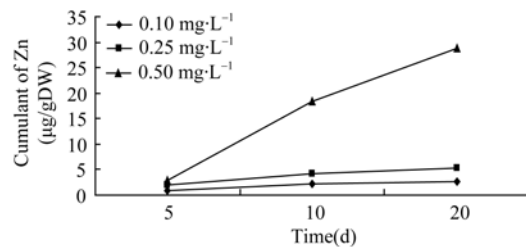


Figure 1 Relationship of accumulation of zinc and time in ovary

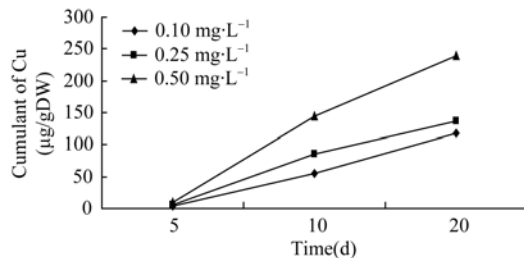


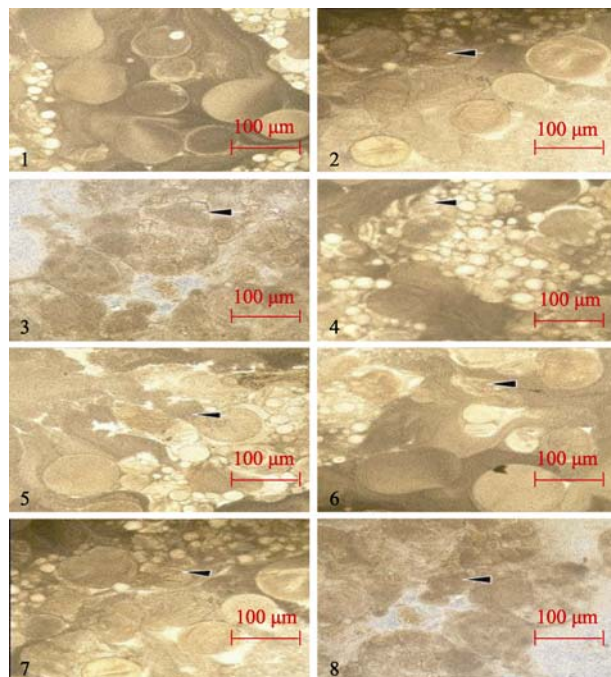
Figure 2 Relationship of accumulation of copper and time in ovary

Stress on ovary development from Zn²⁺ and Cu²⁺

The ovaries and ova in the controls, in which the metals were not detected, developed normally. Zn²⁺ and Cu²⁺ accumulated rapidly in the ovaries of all treatment groups exposed to mixtures of Zn²⁺ and Cu²⁺. The fish showed on the atrophy and cytoplasmic leakage in the ova, suggesting histological damage in the ovaries by day 10 of exposure. By day 20, the ova showed symptoms of severe degeneration, the mutual bonding of cells and severe atrophy (Figure 3).

DISCUSSION

As trace elements of an organism, Zn²⁺ and Cu²⁺ are integral parts of cellular structure and enzyme compounds. Zn²⁺ is one of the important growth factors and plays a vital role in growth, development and appetite, etc. for fishes and other aquatic organisms (Al-Weher S, 2008; Ebrahimi M, 2007). However, studies have shown that higher doses and longer exposure are not beneficial, and have toxic effects on aquatic organisms (Zhou et al, 2002). As for Cu²⁺, it is also a type of nutritive trace element necessary for fish growth (Gao et al, 2003), and it performs important functions for the physiological activities in fishes. The physiological metabolism will be negatively influenced if either Zn²⁺ or Cu²⁺ is lacking, but overdosing brings adverse impacts, especially in the case of Cu²⁺. In general, the harmfulness of Zn²⁺ is relatively small as compared with

Figure 3 Effects of joint attack of Zn²⁺ and Cu²⁺ on ovaries and ova

a: Normal development of ovaries and ova in the control; b: 5 d ovaries and ova, the arrow shows the cell degenerated in group one; c: 10 d ovaries and ova, the arrow shows the cell dehydrated in group one; d: 10 d ovaries and ova, the arrow shows the cell atrophic and dehydrated in group two; e: 10 d ovaries and ova, the arrow shows the cell atrophic and shriveled in group three; f: 20 d ovaries and ova, the arrow shows the cell atrophic and mutual bonding in group one; g: 20 d ovaries and ova, the arrow shows the cell atrophic and mutual bonding in group two; h: 20 d ovaries and ova, the arrow shows the cell atrophic and mutual bonding in group three.

Cu²⁺, which is highly toxic to aquatic organisms in stronger dosages (Wang et al, 2006).

As mentioned above, the amount of Zn²⁺ and Cu²⁺ accumulated in the ovaries was related to the concentration of Zn²⁺ and Cu²⁺ in the aquatic environment and the duration of exposure to the metals. The cumulative amount of heavy metal in the ovaries rises with the concentration of Zn²⁺ and Cu²⁺ to a certain level alongside the exposure period, demonstrating the significant effect of time and doses. However, the accumulation rate tended to decline when exposure time exceeded 10 days. It could be that when organisms are over-exposed to heavy metals such as Zn²⁺ and Cu²⁺, the

metals activate the transcription of metallothionein genes in the organs, resulting in more genes being expressed. Consequently, these expressed genes combine the metals that have entered the cells with those new synthetic proteins (Allen, 1995). Alternatively the cells over-exposed to the heavy metals are in a state of "saturation" and thus can no longer absorb more heavy metals. As exposure continues, the level of heavy metal accumulation declined in the ova, which was more obvious in the cases of different concentrations of Zn²⁺ (Figure 1). As for the accumulation of Cu²⁺ under different concentrations, the higher the concentration of Cu²⁺, the slower the accumulation tended to be. It seemed that the cumulated amount of Cu²⁺ increased in the ova between 10 to 20 days, when the concentration was low, i.e., 0.1 mg/L (Figure 2).

Ultimately, these results indicate that the ability of the ovaries to detoxify decreased and the ova were damaged as a result of 20 day's exposure to heavy metal at higher concentrations. Long term exposure to heavy metals will likely then further damage the overall function of ovaries (Figure 3), which is in agreement with previous studies regarding organs in aquatic organisms being damaged by heavy metals (Wang *et al.*, 2003; Zhang *et al.*, 2009; Zhou *et al.*, 2010).

Our results also showed that when both Zn²⁺ and Cu²⁺ were at a low concentration (1.00 and 0.10 mg/L, respectively), the physiological activities and ovarian development of loaches were not affected by Zn²⁺ and Cu²⁺ within 20 days of exposure, though future studies are needed to determine the effects of long-term exposure at similar concentrations. As the concentration of the metals and/or exposure time increased the function of ovarian development and the metabolism of ova suffered serious damage. Studies of single metal exposure showed that female sword fish (*Xiphophorus Helleri*) on average laid only 17 eggs when exposed to Cu²⁺ (0.12 mg/L) for 140 days, compared with the 228 eggs laid in the control group (James *et al.*, 2003). But the effect of single metal exposure can be very different from multi-metal exposure on aquatic organisms in terms of toxicity accumulation. In a natural environment, a synergic or antagonistic action may occur as different heavy metals usually co-exist (Zhang *et al.*, 2008). In addition, factors such as water temperature, forms of heavy metals, existence of other chemical ions and changes in other environmental variables may affect the heavy metal accumulation and cause harm to aquatic organisms (Li *et al.*, 2002; Tang *et al.*, 2010). Further studies, therefore, are needed to address these issues.

References

Abou El-Naga EH, El-Mosehy KM, Hanmed MA. 2005. Toxicity of cadmium and copper and their effect on some biochemical parameters of marine fish *mugil sheheli*. *Egyptian Journal of Aquatic Resources*, **31**(2): 60-71.

Allen P. 1995. Soft-tissue accumulation of lead in the blue Tilapia, *Oreochromis aureus* (Steindachner) and the modifying effects of cadmium and mercury. *Biological Trace Element Research*, **50**(3): 193-208.

Al-Weher SM. 2008. Levels of heavy metal Cd, Cu and Zn in three fish species collected from the North Jordan Valley, Jordan. *Jordan Journal of Biological Sciences*, **1**(1): 41-46.

da Cruz ACS, Couto BC, Nascimento IA, Pereira SA, Leite MBNL, Bertoletti E, Zagatto P. 2007. Estimation of the critical effect level for pollution prevention based on oyster embryonic development toxicity test: The search for reliability. *Environment International*, **33**(4): 589-595.

Dutta TK, Kavira JA. 2001. Acute toxicity of cadmium to fish *Labeo rohita* and copepod *Diaptomus forbesi* pre-exposed to CaO and KMnO₄. *Chemosphere*, **4**(8): 955-958.

Ebrahimi M. 2007. Effects of *in vivo* and *in vitro* zinc and cadmium treatment on sperm steroidogenesis of the African catfish *Clarias gariepinus*. *Pakistan Journal of Biological Sciences*, **10**(17): 2862-2867.

Gao XL, Qi FS, Luo HY, Wang LM, Li YH. 2003. Acute toxicity and joint toxicity test of Cu, Hg and Cr on *Misgurnus anguillicaudatus*. *Reservoir Fisheries*, **23**(2): 63-64. (in Chinese)

Has Schön E, Bogut I, Kralik G, Bogut S, Horvatić J, Cacić M. 2008.

Heavy metal concentration in fish tissues inhabiting waters of *Busko Blato* reservoir (Bosnia and Herzegovina). *Environment Monitoring Assessment*, **144**(1-3): 15-22.

James R, Sampath K, Edward DS. 2003. Copper toxicity on growth and reproductive potential in an ornamental fish, *Xiphophorus helleri*. *Asian Fisheries Science*, **16**: 317-320.

Li SX, Sun HW, Wang YQ, Dai SG. 2002. Bioconcentration and partition behaviors of tributyltin. *Acta Scientiae Circumstantiae*, **22**(6): 726-731. (in Chinese)

Migliarini B, Campisi A M, Maradonna F, Truzzi C, Annibaldi A, Scarponi G, Carnevali O. 2005. Effects of cadmium exposure on testis apoptosis in the marine teleost *Gobius niger*. *General and Comparative Endocrinology*, **142**(1-2): 241-247.

Nan XY. 2009. Toxicity effects of heavy metals Cu, Zn and Cd and influence to gobble up ability of white blood cells in loach. *Agricultural Science of Shanxi*, **2**: 40-43. (in Chinese)

ang JX, Xing CH, Liu ZL, Cheng ZS, Li JR. 2010. Accumulation of heavy metals (Cu and Pb) in the ovary of *Misgurnus anguillicaudatus* and the subsequent effects on ova development. *Oceanologia et Limnologia Sinica*, **41**(3): 386-390. (in Chinese)

Wang RL, Ma GZ, Fang ZQ. 2006. Safety assessment and acute toxicity of copper, cadmium and zinc to white cloud mountain minnow *tanichthys albonubes*. *Fisheries Science*, **25**(3): 117-120. (in Chinese)

Wang YQ, Zhang YM, Zhao DQ. 2003. Effects of heavy metals cadmium, lead and zinc on the survival of *Carassius auratus* and

misgurnus anguillicaudatus. *Journal of Gansu Sciences*, **15**(1): 35-38. (in Chinese)

Wang YW, Wei YS, Liu JX. 2008. Heavy metal bioaccumulation model of aquatic organisms: An overview. *Acta Scientiae Circumstantiae*, **28**(1): 12-20. (in Chinese)

Zhang HR, Xu XX. 2009. Research on accumulate of heavy metal ions copper and lead in *Cyprinus carpioi juveniles*. *Science and Technology of Food Industry*, **30**(7): 276-278. (in Chinese)

Zhang YM, Wang YJ, Yu RL, Zhou M. 2008. Effects of heavy metals on ATPase and SOD activities of hepatopancreas in *Misgurnus anguillicaudatus*. *Journal of Gansu Sciences*, **20**(3): 55-59. (in Chinese)

Zhou XW, Zhu GN, Sun JH. 2002. Effects of the interaction of heavy metals on the accumulation of copper in the tissues of the fish (*Carassius auratus*). *Journal of Zhejiang University (Agriculture & Life Sciences)*, **28**(4): 427-430. (in Chinese)

Zhou YF, Wu W, You Y, Chen JZ. 2010. Dynamics of metallothionein in organs of *Carassius auratus* under combined stresses of Cd and Zn. *Journal of Ecology and Rural Environment*, **26**(1): 63-67. (in Chinese)

Description of a new *Pratylenchus* species from China (Tylenchida, Pratylenchidae)

Ning LIU, Xiao-Song ZHOU, Li-Jie CHEN, Yu-Xi DUAN*

Nematology Institute of Northern China, Shenyang Agricultural University, Shenyang 110866, China

Abstract: *Pratylenchus ekrami* from maize (*Zea mays*) roots in Shenyang and luffa (*Luffa cylindrica*) roots in Dalian, China, are described in this paper. Nematodes from the two areas were identified consistently, and were characterized by a heavy cephalic sclerotization, extending posteriorly up to two body annuli, stylet 11–13 μm long, elongating conoid tail, and becoming thinner from vulva. Males were not found. *Pratylenchus ekrami* is close to *Pratylenchus vulnus*, but the most critical characteristics between the two species were the number of lip annuli, stylet size, and shape of stylet knobs. This species is the first reported in China.

Keywords: Pratylenchidae; *Pratylenchus*; new record species; *Pratylenchus ekrami*

Root-lesion nematodes of the genus *Pratylenchus* (Bajaj & Bhatti, 1984) rank second only to root-knot and cyst nematodes in terms of worldwide economic impact on crops (Sasser & Freckman, 1987). This is due not only to their wide host range, but also their distribution in almost every cool, temperate and tropical environment. *Pratylenchus* species are obligate biotrophic, soil-inhabiting parasites and are found in all agricultural regions of the world (Hunt & Perry, 2007). So far, more than sixty species in the genus have been recorded (Castillo & Vovlas, 2006). *Pratylenchus ekrami* Bajaj & Bhatti, 1984, belonging to Tylenchida, Pratylenchidae has been recorded only in the soil and roots of *Pyrus malus* L. at a horticultural farm in India. Body of the genus is open C-shaped upon fixation and becomes thinner from the vulva; labial framework is sclerotized, extending posteriorly up to two body annuli; stylet is 11–13 μm long and the tail is conoid (Bajaj & Bhatti, 1984). One species was found from maize (*Zea mays*) roots in Shenyang and luffa (*Luffa cylindrica*) roots in Dalian, China. It was identified as *P. ekrami* after morphological studies, and is reported here for the first time.

MATERIALS AND METHODS

All specimens used in this study were obtained from the soil of maize roots in Shenyang and luffa roots in Dalian, Liaoning Province, which are the first reported occurrences of this species in China. Soil

samples were dissociated by sucrose centrifugation (Chen et al, 2007). Specimens were fixed in FG (8 mL 40% formaldehyde, 2 mL triethanolamine and 90 mL sterile water) for measurement and photographs. First, these specimens were placed on permanent slides. The shape of the females was then observed directly using optical and biological microscopes. The fine structure was observed by using an oil immersion lens. Photographs were taken and features were measured using motic metrology software. Good photos were selected to be drawn.

RESULTS

Pratylenchus ekrami Bajaj & Bhatti, 1984, a new record species in China (Figure 1).

Measurements

Female ($n=10$): $L=422.0\text{--}490.0$ (449.9 ± 25.20) μm , $W=13.7\text{--}20.2$ (16.9 ± 2.43) μm , $a=21.7\text{--}33.3$ (26.4 ± 4.46), $b=5.2\text{--}6.7$ (6.03 ± 0.47), $b'=3.4\text{--}5.2$ (4.5 ± 0.85), $c=15.3\text{--}22.6$ (18.88 ± 2.34), $c'=1.6\text{--}2.2$ (1.83 ± 0.26), $V=79.9\%\text{--}83\%$ (81.58 ± 1.07), stylet= $11.2\text{--}13.1$ (12.23 ± 0.74) μm , Tail= $18.7\text{--}28.3$ (23.48 ± 3.13) μm .

Received: 05 March 2013; Accepted: 15 June 2013

Foundation item: This work was supported by China Agriculture Research System (CARS-04)

*Corresponding author, E-mail: duanyx6407@163.com

L: body length; *W*: greatest body width; *a*: body length/greatest body width; *b*: body length/distance from anterior end to junction of oesophagus and intestine; *b'*: body length/distance from anterior end to oesophagus end; *c*: body length/tail length; *c'*: tail length/anus body width; *V*: distance from vulva to anterior end \times 100/body length.

Description

Female: Body opened C-shaped upon fixation. The body became slender from vulval region. Lateral fields with four lines extended to tail terminus. Labial region was continuous with the rest of the body, anteriorly

truncate, and had three annules. Labial framework was sclerotized, extending posteriorly up to two body annuli. Stylets were 11–13 μm long with rounded, sloping knobs. Corpus was long, almost cylindrical. Median bulb was oval. Pharyngeal gland overlapped the intestine. Opening of dorsal was 3–4 μm from stylet base. Nerve ring was located at mid-isthmus. Excretory pore was 74–79 μm from anterior extremity. Hemizonid was just anterior to excretory pore. Spermatheca was elongated oval and filled with sperm. Vulva was a transverse slit located at 77%–83% of body length. Tail was elongated conoid or blunt.

Male: Not found.

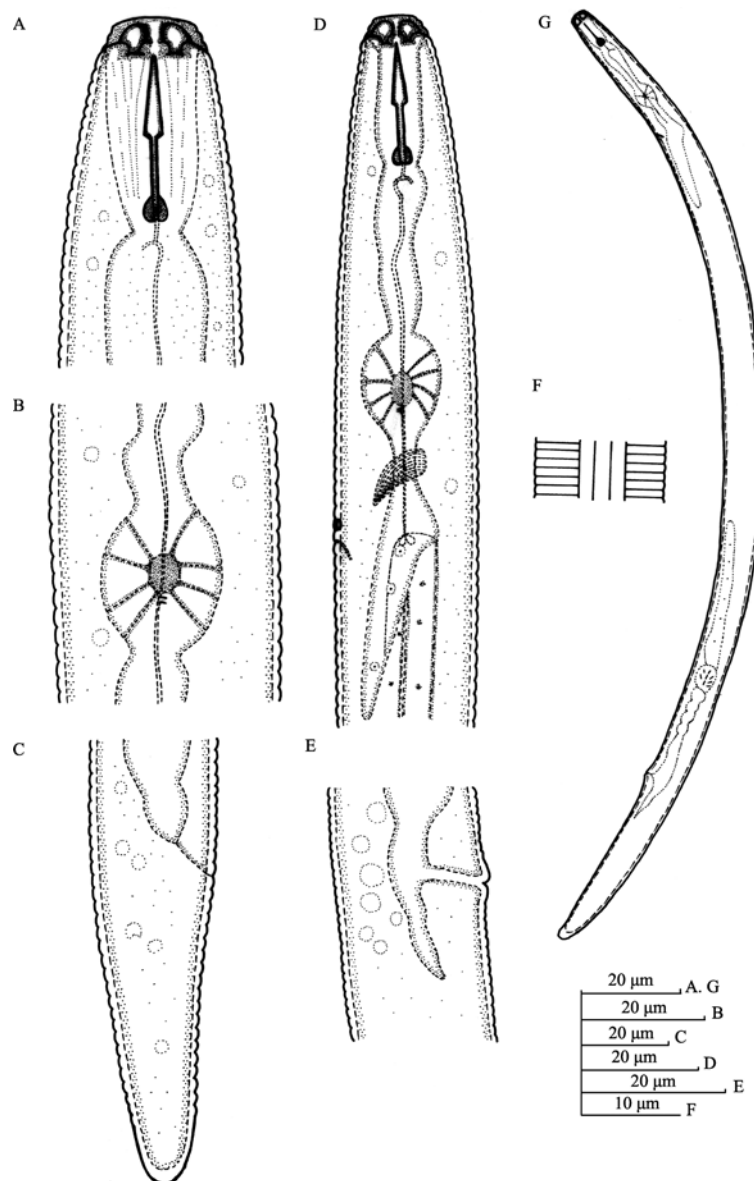


Figure 1 Illustrations of *Pratylenchus ekrami*

A: Female pharyngeal region; B: Tail of female; C: Female labial region; D: Female esophageal bulb region; E: Female vulvar region; F: Lateral field; G: Entire female.

DISCUSSION

Pratylenchus ekrami was close to *Pratylenchus vulnus*, although they differed in shape of labial region, number of lip annuli, stylet size, shape of stylet knobs and median bulb, details of lateral lines and number of tail annuli. *Pratylenchus ekrami* is characterized by: labial region continuous with rest of body, anteriorly truncate, three

annuli, stylet 11–13 μm long with rounded, sloping knobs, tail tip narrowly to broadly rounded. The characteristics of *P. vulnus* are labial region high, lip annuli usually three or four on one side and four on the other, stylet 14–18 μm long, stylet knobs rounded, central band of lateral lines narrower than outer ones, median bulb oval, relatively narrow.

References

Bajaj HK, Bhatti DS. 1984. New and known species of *Pratylenchus* Filipjev, 1936 (Nematoda: Pratylenchidae) from Haryana, India, with remarks on intraspecific variations. *Journal of Nematology*, **16**(4): 360–367.

Castillo P, Vovlas N. 2006. *Pratylenchus* (Nematoda: Pratylenchidae): Diagnosis, Biology, Pathogenicity and Management // Hunt DJ, Perry RN. Nematology Monographs and Perspectives. Vol. 1. Leiden: Brill Publishing, 65–75.

Chen LJ, Wang X, Duan YX, Sun XM. 2007. Extraction effectiveness of soil nematodes with sucrose-centrifugation method. *Journal of Shenyang Agricultural University*, **38**(6): 849–851.

DE MAN, J.G. (1880). Die Einheimischen, frei in der reinen Erde und im süßen Wasser lebenden Nematoden. Vorläufiger Bericht und descriptive-systematischer Teil. *Tijdschrift der Nederlandse Dierkundige Vereeniging*, 5: 1–104.

Hunt DJ, Perry RN. 2007. *Pratylenchus* (Nematoda: Pratylenchidae): Diagnosis, Biology, Pathogenicity and Management. In: Hunt DJ, Perry RN. Nematology Monographs and Perspectives. Leiden: Brill Publishing, 112–114.

Sasser JN, Freckman DW. 1987. A world perspective on Nematology: the role of the society. In: Veech JA, Dickson DW. *Vistas on Nematology*. Hyattsville, MD, USA: Society of Nematologists, 7–14.

ZOOLOGICAL RESEARCH EDITORIAL BOARD

Advisors: Yi-Yu CHEN Ru-Yong SUN Wen-Ying YIN Er-Mi ZHAO Guang-Mei ZHENG

Honorary Editor-in-Chief: Ya-Ping ZHANG

Editor-in-Chief: Yong-Gang YAO

Executive Editor-in-Chief: Yong-Tang ZHENG

Associate Editors-in-Chief: Le KANG Chungi WU Jing-Xia CAI Ying-Xiang WANG

Yun ZHANG Bing-Yu MAO

Members:

Adel AB Shahin Bin LIANG Boris Vyskot Ce-Shi CNEN Ding-Qi YAO Hong-Wen DENG Ping DING

Eske Willerslev Frederick C Leung Jing-Fei HUANG Igor Khorozyan Wei-Zhi JI Xiang JI Xue-Long JIANG

Ren LAI Sang-Hong LEE Dai-Qin LI Qing-Wei LI Huan-Zhang LIU Jie MA Yuan-Ye MA Michael H Ferkin

Nallar B Ramachandra Natchimuthu Karmegam Neena Singla Nicolas Mathevon Pim Edelaar

Prithwiraj Jha Radovan Vaclav Bing SU Tibor Vellai Vallo Tilgar Walter Salzburger Wen WANG

Xiao-Ming WANG Yi-Quan WANG Yue-Zhao WANG Fu-Wen WEI Jian-Fan WEN Rong-Ling WU

Xiao-Bing WU Heng XIAO Lin XU Jun-Xing YANG Guang YANG Xiao-Jun YANG Xiao-Yong CHEN

Gen-Hua YUE Hua-Tang ZHANG Yan-Yun ZHANG Ya-Jun ZHAO Rong-Jia ZHOU Wei ZHOU

Editors: Long NIE Su-Qing LIU Fang SHAN

Editor for English Language and Design: Andrew T Willden

Edited by Editorial Office of Zoological Research

(Kunming Institute of Zoology, the Chinese Academy of Sciences, 32 Jiaochang Donglu, Kunming,

Yunnan, Post Code: 650223 Tel: +86 871 65199026 Fax: +86 871 65113532

E-mail: zoores@mail.kiz.ac.cn Website: <http://www.zoores.ac.cn>)

Editor-in-Chief: Yong-Gang YAO

Sponsored by Kunming Institute of Zoology, the Chinese Academy of Sciences; China Zoological Society©

Published by Science Press (16 Donghuangchenggen Beijie, Beijing 100717, China)

Printed by Kunming Xiaosong Plate Making & Printing Co, Ltd

Domestic distribution by Yunnan Post and all local post offices in China

International distribution by China International Book Trading Corporation (Guoji Shudian) P.O.BOX 399,
Beijing 100044, China